CircRAD18 promotes glioblastoma proliferation, migration and invasion via the miR-1231/LUC7L2 axis

LUMENG SONG[1*], PING XIONG[1*], AMU JIKE[1*], XIAOCHAO XIA[1], LIFANG MAO[2], ZIHAO WANG[1], YINCHUAN CHENG[1], SHUMIN WANG[1], SHIZHENG TAN[1], DONGNAN YU[1], ZHENG LI[1], XIAOPING TANG[1,3] and SHUN LI[1,3]

[1]Department of Neurosurgery, Affiliated Hospital of North Sichuan Medical College, Nanchong, Sichuan 637000, P.R. China; [2]Nursing Department, Affiliated Hospital of North Sichuan Medical College, Nanchong, Sichuan 637000, P.R. China; [3]Department of Neurosurgery, Neurosurgical Research Center, Affiliated Hospital of North Sichuan Medical College, Nanchong, Sichuan 637000, P.R. China

Received July 24, 2025; Accepted April 1, 2026

DOI: 10.3892/ijmm.2026.5851

Abstract. Glioblastoma (GBM) is an exceptionally aggressive and malignant central nervous system tumor with a poor prognosis. Studies suggest that circular RNAs (circRNAs) play a vital role in GBM progression. Exosomes, key mediators of intercellular communication, carry circRNAs that may regulate this process. The present study aimed to investigate how circRAD18 modulates GBM cell proliferation, migration and invasion through the miR-1231/LUC7L2 axis and to evaluate the potential of exosomal circRAD18 as a diagnostic biomarker for GBM. Bioinformatics analyses identified differentially expressed circRAD18, miR-1231 and LUC7L2 in GBM and predicted their interactions. Expression levels were assessed using western blot analysis, immunohistochemistry and reverse transcription-quantitative polymerase chain reaction. Regulatory mechanisms were examined via dual-luciferase reporter assays, RNA pull-down assays, CCK-8 assays, wound healing assays, Transwell assays, fluorescence *in situ* hybridization and subcutaneous xenograft tumor models in nude mice. Exosomes were isolated by ultracentrifugation and characterized using transmission electron microscopy and nanoparticle tracking analysis. circRAD18 expression was markedly upregulated in GBM samples and cell lines. Knockdown of circRAD18 markedly inhibited GBM cell proliferation, migration and invasion both *in vitro* and *in vivo*. Suppression of miR-1231 or overexpression of LUC7L2 enhanced GBM cell proliferation, migration and invasion *in vitro*, but these effects were counteracted by simultaneous circRAD18 knockdown. Additionally, exosomes derived from GBM cells contained high levels of circRAD18. circRAD18 promotes GBM proliferation, migration and invasion by regulating the miR-1231/LUC7L2 axis. Given its substantial expression in GBM-derived exosomes, circRAD18 holds promise as both a therapeutic target and a diagnostic biomarker for GBM.

Correspondence to: Professor Shun Li or Professor Xiaoping Tang, Department of Neurosurgery, Affiliated Hospital of North Sichuan Medical College, 1 Maoyuan South Road, Shunqing, Nanchong, Sichuan 637000, P.R. China
E-mail: bertlee120@163.com
E-mail: txping1971@163.com

*Contributed equally

Abbreviations: GBM, glioblastoma; CNS, central nervous system; circRNAs, circular RNAs; ncRNAs, non-coding RNAs; miRNA, microRNA; 3'UTR, 3'untranslated region; NBTs, normal brain tissues; WHO, World Health Organization; DMEM, Dulbecco's modified Eagle's medium; FBS, fetal bovine serum; si, small interfering RNA; NC, negative control; shRNA, short hairpin RNA; RT-qPCR, reverse transcription-quantitative polymerase chain reaction; RNase R, ribonuclease R; FISH, fluorescence *in situ* hybridization; PBS, phosphate-buffered saline; SSC, saline-sodium citrate; DAPI, 4,6-diamidino-2-phenylindole; CCK-8, cell counting kit-8; IHC, immunohistochemistry; TEM, transmission electron microscopy; PTA, phosphotungstic acid; NTA, nanoparticle tracking analysis; GEO, Gene Expression Omnibus; CGGA, Chinese Glioma Genome Atlas; SEM, standard error of the mean; EVs, extracellular vesicles; VEGFA, vascular endothelial growth factor A

Key words: glioblastoma, circRAD18, miR-1231, LUC7L2, exosomes

Introduction

Glioblastoma (GBM) accounts for 50.1% of central nervous system (CNS) malignancies, making it the predominant and most fatal primary CNS tumor. The median survival time for individuals with GBM is ~eight months and the five-year survival rate is only 6.9% (1). The current treatment for GBM primarily relies on surgical extraction of the tumor, combined with radiation therapy and chemotherapy. Nevertheless, the highly invasive and heterogeneous nature of GBM makes complete resection challenging. Combined with significant resistance to both chemotherapy and radiotherapy, the patient's prognosis remains extremely poor (2). Therefore, investigating the mechanisms underlying GBM and identifying new targets for therapy is of significant clinical value.

With a covalently closed loop structure, circular RNAs (circRNAs) are a subclass of non-coding RNAs (ncRNAs). RNA polymerase II back-splices precursor mRNA to create circRNAs (3). As circRNAs lack a 5'cap structure and a 3'polyadenylated tail, they are resistant to degradation by RNA exonucleases, ensuring their stable expression in cells (4). circRNAs play a critical role in the pathogenesis of several diseases, including neurological, cardiovascular, digestive and reproductive disorders (5). Some studies suggest that circRNAs regulate the onset and progression of disease by acting as microRNA (miRNA) sponges (6-8). This involves binding to miRNA sites and adjusting the expression of the genes that miRNAs target (9). miRNAs are a class of small (~22 nucleotides), single-stranded endogenous ncRNAs that bind to the 3'untranslated region (3'UTR) of target mRNAs to regulate gene expression (10-12). For example, circ_0006528 enhances the level of chromodomain helicase DNA binding protein 4 expression and promotes breast cancer cell proliferation by acting as a sponge for miR-1236-3p (13). Additionally, circRNAs can bind to chromatin, mRNA, or circRNA binding proteins, regulating processes such as protein translocation, mRNA stability, protein translation and gene transcription (9,14). Recent research has shown that circRNAs are essential for GBM processes such as angiogenesis, migration, invasion, treatment resistance and proliferation, impacting tumor development (15). For example, Li *et al* (16) discovered that circARID1A controls the miR-370-3p/TGFBR2 pathway to encourage GBM cell migration and invasion. Thus, investigating the role of circRNAs in GBM development and progression has important theoretical implications and potential therapeutic applications.

Numerous human cells produce exosomes, which are nanometer-sized extracellular vesicles (EVs) (17) found in bodily fluids such as blood, amniotic fluid, breast milk and semen (18,19). Exosomes generated from tumor cells have been shown to contain metabolites, membrane proteins, nuclear proteins, nucleic acids and other components, contributing to intercellular communication (20,21). These exosomes interact with stromal cells within the tumor microenvironment, thereby influencing tumor proliferation, invasion, angiogenesis, immunosuppression and drug resistance (20,22,23). For example, Zhang *et al* (24) found that glioma cells transferred markedly upregulated circRNA_104948 to normal astrocytes via exosomes, upregulating the expression of the oncogenic factor DNMT3B and decreasing the expression of the tumor suppressor MTSS1 by sponging miR-29b-3p, ultimately promoting the over-proliferation of astrocytes. Therefore, investigating glioma cell-derived exosomes could provide new insights into the mechanisms underlying glioma occurrence and development, as well as the development of diagnostic markers.

circRAD18 (hsa_circ_0001264) was revealed to be markedly expressed in GBM cells using bioinformatics research. It also acts as a sponge for miR-1231, indirectly controlling LUC7L2 expression. Through its regulation of the miR-1231/LUC7L2 axis, circRAD18 has been shown in both *in vitro* and *in vivo* experiments to enhance GBM development. Additionally, circRAD18 was highly enriched in GBM cell-derived exosomes. In the present study, a novel circRNA in the development and progression of GBM is revealed, pointing to possible therapeutic targets and diagnostic markers.

Materials and methods

Clinical specimens. A total of 74 GBM tissue samples were retrospectively collected and analyzed from patients who underwent surgical resection at the Affiliated Hospital of North Sichuan Medical College (Nanchong, Sichuan, China) between September 2022 and March 2024. The cohort included 45 male and 29 female patients, with an age range of 40-80 years. Diagnosis was established by senior associate chief physicians and chief physicians in the pathology department based on typical histopathological features of GBM according to the World Health Organization (WHO) Classification of Tumors of the CNS, 5th edition (2021) (25). As part of routine pathological evaluation, immunohistochemical analyses, including glial fibrillary acidic protein, oligodendrocyte transcription factor 2, Ki-67 proliferation marker, tumor protein p53 (p53), α-thalassemia/mental retardation syndrome X-linked and isocitrate dehydrogenase 1 (IDH1; R132H), were performed. Notably, all 74 cases were confirmed as IDH-wildtype based on IDH1 immunohistochemistry and exhibited characteristic histopathological features of GBM, such as microvascular proliferation and/or necrosis. No IDH-mutant astrocytomas were included in the cohort. In addition, molecular pathological testing was performed in 32 patients as part of routine clinical evaluation. All four molecular assays, including O6-methylguanine-DNA methyltransferase promoter methylation, telomerase reverse transcriptase promoter mutation, epidermal growth factor receptor (EGFR) amplification and combined chromosome 7 gain/chromosome 10 loss (+7/-10), were completed for all 32 patients. However, as the diagnosis for the entire cohort was already definitively established through the integrated IDH-wildtype status and histopathological hallmarks, these additional molecular data were not used as inclusion criteria for the present study. None of the tumors met WHO 2021 GBM diagnostic criteria based on molecular features alone, because all cases showed grade 4 histopathological hallmarks. Inclusion criteria were as follows: i) Patients with a primary diagnosis of GBM confirmed by histopathological examination; ii) availability of sufficient tumor tissue for subsequent analyses; and iii) complete clinical and pathological information. Exclusion criteria included: i) Recurrent GBM; ii) prior chemotherapy or radiotherapy before surgical resection; and iii) insufficient or poor-quality tissue samples unsuitable for analysis. Additionally, adjacent normal brain tissues (NBTs) were collected from 21 patients with GBM and used as normal controls. All surgical resections were performed by senior neurosurgeons with extensive clinical experience. NBTs were obtained from regions located at least 2 cm away from the tumor margin, ensuring accurate intraoperative differentiation between tumor tissue and non-tumoral brain tissue. The collected adjacent samples were evaluated microscopically by senior associate chief physicians and chief physicians in the pathology department using standard hematoxylin and eosin (H&E) staining. The absence of tumor infiltration was determined based on established histological criteria, including the absence of hypercellularity, nuclear atypia, mitotic figures, microvascular proliferation, or

necrosis. Only tissues judged to be free of overt tumor infiltration were included as NBT controls. Notably, no molecular or genetic testing was performed to further confirm the absolute normality of these adjacent tissues, which remains a limitation of the current study. All enrolled patients and their families provided informed consent. The study was approved by the Clinical Ethics Committee of the Affiliated Hospital of North Sichuan Medical College (approval no. 2024020).

Cell lines and cell culture. Human GBM cell lines (U87, U251, A172 and T98G) were obtained from Keycell Biotech (Wuhan) Co., Ltd. (cat. nos. U87-QS-H103, U251-QS-H007, A172-QS-H021 and T98G-QS-H034). The HA1800 astrocyte cell line was supplied by Xiamen Immocell Biotechnology Co., Ltd. (cat. no. HA1800-IM-H437). The U87 cell line corresponds to the U87 MG ATCC version (cat. no. HTB-14) and its precise origin is unknown. The identity of the U87 cell line was authenticated by STR profiling prior to use. The cells were cultured in Dulbecco's Modified Eagle's Medium (DMEM; Keycell Biotech (Wuhan) Co., Ltd.), supplemented with 10% fetal bovine serum (FBS; INTL KANG) and 1% penicillin-streptomycin solution [Keycell Biotech (Wuhan) Co., Ltd.]. The cells were then incubated at 37˚C in a humidified incubator with 5% CO_2 (Shanghai Yiheng Technology Co., Ltd.).

Transfections. The small interfering RNAs (siRNAs) investigated in the present study included si1-circRAD18, si2-circRAD18, circRAD18-negative control (NC), miR-1231 mimic, miR-1231 mimic NC, miR-1231 inhibitor and miR-1231 inhibitor NC, all designed and synthesized by General Biosystems (Anhui) Co., Ltd. The siRNAs targeting circRAD18 were specifically designed against the back-splice junction sequence unique to circRAD18. The mature sequence of miR-1231 was 5'-GUGUCU GGGCGGACAGCUGC-3'. The LUC7L2 overexpression plasmid VP051-CMV-MCS-EF1-ZsGREEN-T2A-PURO (OE-LUC7L2) and its corresponding empty vector (OE-NC) were constructed by Wuhan Huibao Bio-Technology Co., Ltd. U87 and U251 cell lines were used for transfection. In 96-well plates, cells in the logarithmic growth phase with optimal viability were plated at a density of $5x10^3$ cells per well and incubated overnight at 37˚C in a 5% CO_2 incubator. Transfection was performed when the cells reached 80% confluency. For each well, 0.5 μl of si1-circRAD18, si2-circRAD18, circRAD18-negative control (NC), miR-1231 mimic, miR-1231 mimic NC, miR-1231 inhibitor or miR-1231 inhibitor NC at a concentration of 20 μM was used for transfection. According to the manufacturer's instructions, Lipofectamine® 2000 (Invitrogen; Thermo Fisher Scientific, Inc.) was used to transfect the cells. Subsequent experiments were performed 48 h after transfection. Short hairpin RNAs (shRNAs), including sh1-circRAD18, sh2-circRAD18 and sh-circRAD18-NC, were produced by Wuhan Bio-Tower Biotechnology Co., Ltd. The pLVX-ShRNA2-Puro plasmid (Wuhan Bio-Tower Biotechnology Co., Ltd.) was used to construct a shRNA expression vector. An empty vector lacking the circRAD18 sequence was used as an NC. To produce lentiviruses, co-transfection of the shRNA expression vector (10 μg) and the packaging plasmids (15 μg) was performed in 293T cells from Keycell Biotech (Wuhan) Co., Ltd. when the cells reached 80% confluency. For lentiviral infection, U87 cells were plated in 6-well plates at a density of $5x10^4$ cells per well and cultured in complete medium overnight. A viral suspension with a multiplicity of infection of five was added to each well and incubated at 37˚C. At 48 h after infection, the culture medium was replaced with fresh medium containing 2 μg/ml puromycin (Shanghai Yuanye Bio-Technology Co., Ltd.) for selection of stably transduced cells. The medium was changed every two to three days to remove dead cells and maintain selective pressure until stable transduction was indicated by the formation of resistant colonies. Subsequently, stably transduced cells were maintained in medium containing 2 μg/ml puromycin for routine culture. Table I lists the oligonucleotide sequences used for cell transfection.

Reverse transcription-quantitative (RT-q) PCR. TRIzol® reagent (Invitrogen; Thermo Fisher Scientific, Inc.) was used to extract RNA from tissues and cell lines according to the manufacturer's protocol. For cell samples, RNA was extracted from $1x10^6$ cells. HiScript® II Q Select RT SuperMix for qPCR (Vazyme Biotech Co., Ltd.) was used to reverse-transcribe circRAD18 and LUC7L2 mRNA into cDNA after RNA concentration and purity were assessed, according to the manufacturer's protocol. The miRNA 1st Strand cDNA Synthesis Kit (by tailing A; Vazyme Biotech Co., Ltd.) was used to reverse-transcribe miR-1231 according to the manufacturer's protocol. The cDNA was mixed with 2X Q3 SYBR qPCR Master Mix (ToloBio) for RT-qPCR, which was performed using specific primers on a ViiA 7 Real-Time PCR System (Applied Biosystems; Thermo Fisher Scientific, Inc.) in accordance with the manufacturer's instructions. The thermocycling conditions were as follows: Initial denaturation at 95˚C for 10 min, followed by 40 cycles of denaturation at 95˚C for 10 sec and annealing/extension at 60˚C for 60 s. Subsequently, melting curve analysis was performed by heating at 95˚C for 15 sec, cooling to 60˚C for 60 sec and reheating to 95˚C for 15 sec to verify amplification specificity. All experiments were performed with three independent biological replicates, and each sample was analyzed in triplicate. Relative gene expression was calculated using the $2^{-\Delta\Delta Cq}$ method (26), with GAPDH, β-actin and U6 as internal controls. The reverse primers for miR-1231 were purchased from Vazyme Biotech Co., Ltd. and other primers are listed in Table II.

Ribonuclease R (RNase R) treatment and specific primer amplification assay. Total RNA and genomic DNA (gDNA) were extracted from U87 cells using TRIzol® reagent (Invitrogen; Thermo Fisher Scientific, Inc.) and a universal gDNA kit [Tiangen Biotech (Beijing) Co., Ltd.]. A total of 5 μg of RNA was collected and RNase R-treated and mock-treated groups were established. The cells were treated with 20 U/μl of RNase R (IVDShow Biotechnology Huailai Co., Ltd.) for 30 min at 37˚C. A 20 μl reaction system was prepared as follows: Template RNA (2.5 μg), 10X Reaction Buffer (2 μl), RNase R (2 μl) and RNase-free ddH_2O (adjusted to a final volume of 20 μl). Following reverse transcription, RT-qPCR was performed using convergent and divergent primers. The amplified products were then analyzed using agarose gel

Table I. Oligonucleotide sequences used for cell transfection assays.

Name	Sense (5'→3')	Antisense (3'→5')
circRAD18-NC	UUCUCCGAACGUGUCACGUTT	ACGUGACACGUUCGGAGAATT
si1-circRAD18	AUCAGGAAUCAUCUGCUGCTT	GCAGCAGAUGAUUCCUGAUTT
si2-circRAD18	CAGGAAUCAUCUGCUGCAGTT	CUGCAGCAGAUGAUUCCUGTT
miR-1231 mimic NC	UCACAACCUCCUAGAAAGAGUAGA	UCUACUCUUUCUAGGAGGUUGUGA
miR-1231 mimic	GUGUCUGGGCGGACAGCUGC	GCAGCUGUCCGCCCAGACAC
miR-1231 inhibitor NC	UCUACUCUUUCUAGGAGGUUGUGA	
miR-1231 inhibitor	GCAGCUGUCCGCCCAGACAC	
sh1-circRAD18 #1	GATCCGCGCGAAGAGAAGAAGGAAATTCA AGAGATTTCCTTCTTCTCTTCGCGTTTTTG	
sh1-circRAD18 #2	AATTCAAAAACGCGAAGAGAAGAAGGAAA TCTCTTGAATTTCCTTCTTCTCTTCGCGCG	
sh2-circRAD18 #1	GATCCGGATTATCTATTCAAGGAATTCAAGA GATTCCTTGAATAGATAATCCTTTTTTG	
sh2-circRAD18 #2	AATTCAAAAAAGGATTATCTATTCAAGGAAT CTCTTGAATTCCTTGAATAGATAATCCG	

circ, circular RNAs; miRNA, microRNA; sh, short hairpin RNA; NC, negative control.

Table II. Primer sequences for reverse transcription-quantitative PCR.

Primer name	Sequences
circRAD18 forward primers	AGAAGAAGGAAAGCCTCAGAAGT
circRAD18 reverse primers	AAGCAGGAGATTTGGCTGGTGAC
linear RAD18 forward primers	AAGCAGGGGAGCAGGTTAAT
linear RAD18 reverse primers	TAGCCTCTGAGGGATCTGGA
miR-1231 forward primers	TGCGCGTGTCTGGGCGGACA
miR-1231 reverse primers	GTCGTATCCAGTGCAGGGTCCGAGGT ATTCGCACTGGATACGACGCAGCTGT
LUC7L2 forward primers	CTGAAGGGAATGTGGAGGAA
LUC7L2 reverse primers	GCAGTTTACCCCCAAAATGA
GAPDH forward primers	TCAAGAAGGTGGTGAAGCAGG
GAPDH reverse primers	TCAAAGGTGGAGGAGTGGGT
β-actin forward primers	CCCTGGAGAAGAGCTACGAG
β-actin reverse primers	CGTACAGGTCTTTGCGGATG
U6 forward primers	CGCTTCGGCAGCACATATAC
U6 reverse primers	AAATATGGAACGCTTCACGA

circ, circular RNAs; miRNA, microRNA.

electrophoresis. Table III lists the sequences of the primers, which were acquired from Beijing Tsingke Biotech Co., Ltd.

Fluorescence in situ hybridization (FISH). Cell climbing slides were used for FISH. Following a 20-min fixation in 4% paraformaldehyde [Keycell Biotech (Wuhan) Co., Ltd.] at room temperature, the cells underwent three 5-min washes with phosphate-buffered saline [PBS; Keycell Biotech (Wuhan) Co., Ltd.]. The slides were permeabilized with proteinase K (20 μg/ml) (Wuhan Servicebio Technology Co., Ltd.) for 2 min. After digestion, the slides were given three 5-min rinses with distilled water, followed by three 5-min washes with PBS. The slides were pre-hybridized by incubating them for 1 h at 37˚C in pre-hybridization buffer. The hybridization buffer containing the first probe was used to perform the hybridization, which was then incubated overnight at 37˚C in a humidified chamber. Post-hybridization washes were conducted with saline-sodium citrate (SSC) buffer (Wuhan Servicebio Technology Co., Ltd.) at 37˚C, using the following steps: 2XSSC for 10 min, 1XSSC for 5 min twice and 0.5XSSC for 10 min. If non-specific hybridization occurred, an additional formamide wash was performed. The procedure was repeated for the second probe with the

Table III. Primer sequences for specific primer amplification assay.

Primer name	Sequences
circRAD18 forward primers (Divergent primer)	AGAAGAAGGAAAGCCTCAGAAGT
circRAD18 reverse primers (Divergent primer)	AAGCAGGAGATTTGGCTGGTGAC
linear RAD18 forward primers (Convergent primer)	AAGCAGGGGAGCAGGTTAAT
linear RAD18 reverse primers (Convergent primer)	TAGCCTCTGAGGGATCTGGA

circ, circular RNAs.

Table IV. Probes for fluorescence *in situ* hybridization.

Primer name	Sequences
circRAD18	GGAACGAATGAGTTCAGTGCAACG
miR-1231	GTGTCTGGGCGGACAGCTGC

circ, circular RNAs; miRNA, microRNA.

same pre-hybridization, hybridization and post-hybridization steps. After hybridization, 4,6-diamidino-2-phenylindole (DAPI; Beyotime Biotechnology) was used to counterstain the nuclei for 5 min in the dark. This was followed by washing and mounting with an anti-fade medium. An Olympus fluorescence microscope (Olympus Corporation) was used to observe and photograph the slides. All FISH probes used in the present study were commercially designed and synthesized by Sangon Biotech Co., Ltd. as 5'-Cy3-labeled oligonucleotide probes. The circRAD18 probe was 24 nt in length, and the miR-1231 probe was 20 nt in length. The probe sequences are listed in Table IV.

Cell counting kit-8 (CCK-8) assay. A 96-well plate was used to culture the transfected cells at a density of $5x10^3$ cells per well. After that, the medium was mixed with 10 μl of CCK-8 reagent [Keycell Biotech (Wuhan) Co., Ltd.] and incubated for 1 h. The absorbance of the cells at 450 nm at 24, 48 and 72 h after transfection was then measured using a microplate reader (BIOBASE). Cell viability was evaluated by analyzing these data.

Wound healing assay. Initially, U87 and U251 cell lines were plated at $1x10^6$ cells/well until confluent on 6-well plates. Next, a 200-μl pipette tip was used to make uniformly sized scratches in the cell monolayers. Each wound was imaged at 0, 12 and 24 h using an inverted microscope (Nikon Corporation) following cell washing with PBS to eliminate fragmented cellular debris. During the wound healing assay, the cells were maintained in serum-free DMEM [Keycell Biotech (Wuhan) Co., Ltd.]. No drugs were used in this assay.

Transwell assay. The Transwell assay involved applying 100 μl of Matrigel (1 mg/ml; Corning, Inc.) to the upper chamber of the insert and incubating it for 1 h at 37˚C. The upper chamber was used to seed glioma cells in the exponential growth phase. DMEM [Keycell Biotech (Wuhan) Co., Ltd.] was applied to the upper and lower chambers, together with 10% FBS (INTL KANG) and 1% penicillin-streptomycin [Keycell Biotech (Wuhan) Co., Ltd.]. The cells in the lower chamber were fixed with 70% ice-cold ethanol for 1 h and then stained with 0.5% crystal violet (Wuhan Servicebio Technology Co., Ltd.) at room temperature for 20 min. The number of invasive glioma cells was counted using an inverted microscope (Nikon Corporation).

Western blot analysis. Total protein was extracted from cells using RIPA lysis buffer supplied by Wuhan Servicebio Technology Co., Ltd. Protein concentration was measured using a BCA test kit (GBCBIO Technologies Inc.). Standard protocols were followed to separate equivalent amounts of protein (40 μg per lane) using 5% stacking gel and 10, 12 or 15% separating gels, depending on the molecular weight of the target protein, and transfer them onto PVDF membranes (MilliporeSigma). The membranes were blocked for 2 h at room temperature using 5% skimmed milk and then incubated with the primary antibodies overnight at 4˚C. The next day, the membranes were incubated for 2 h at room temperature after secondary antibodies were added. ECL substrate (Wuhan Servicebio Technology Co., Ltd.) was then used to visualize the protein bands and capture the image. Densitometric analysis was performed using Image-Pro Plus software (version 6.0.0.260; Media Cybernetics, Inc.). Details of the primary and secondary antibodies, including their dilutions, are provided in Table V.

Dual-luciferase reporter assay. For the construction of the luciferase reporter gene, the 3'UTR sequences of circRAD18 or LUC7L2 containing the predicted and mutated binding sites were inserted into the psiCHECK-2 vector (BIOFENG). The constructs included circRAD18-WT, circRAD18-MUT, LUC7L2 3'UTR-WT and LUC7L2 3'UTR-MUT. Then, using Lipofectamine® 2000 (Invitrogen; Thermo Fisher Scientific, Inc.), the luciferase reporter gene was co-transfected into U87 cells with either a miR-1231 mimic or a miR-1231 mimic NC. The cells were incubated at 37˚C in a 5% CO_2 incubator, and the medium was replaced with normal culture medium after 6 h. After 48 h of transfection, the dual-luciferase reporter gene assay kit (Beyotime Biotechnology) was used to quantify luciferase activity according to the manufacturer's instructions.

RNA pulldown assay. Sangon Biotech Co., Ltd. synthesized the biotin-labeled circRAD18 and NC probes. RNA pull-down was performed using the RNA-Binding Protein Immunoprecipitation Kit (MilliporeSigma). U87 cells were collected by centrifugation at 215 x g for 5 min at 4˚C and then lysed. The lysates were centrifuged at 18,757 x g for 10 min

Table V. Information on antibodies used in the present study.

Reagent	Source	Cat. no.	Dilution
Mouse monoclonal anti-β-actin	Affinity Biosciences, Ltd.	T0022	1:20,000
Rabbit polyclonal anti-MMP2	BIOSS	bs-4599R	1:500
Rabbit polyclonal anti-MMP9	Proteintech Group, Inc.	10375-2-AP	1:1,500
Rabbit polyclonal anti-MMP14	Proteintech Group, Inc.	14552-1-AP	1:1,500
Rabbit polyclonal anti-N-cadherin	Affinity Biosciences, Ltd.	AF4039	1:600
Rabbit polyclonal anti-vimentin	Proteintech Group, Inc.	10366-1-AP	1:5,000
Rabbit polyclonal anti-LUC7L2	Proteintech Group, Inc.	24202-1-AP	1:1,500
Rabbit polyclonal anti-CD9	Affinity Biosciences, Ltd.	AF5139	1:1,000
Rabbit polyclonal anti-CD63	Affinity Biosciences, Ltd.	DF2305	1:1,000
HRP-conjugated goat anti-rabbit secondary antibody	Beyotime Biotechnology	A0208	1:1,000
HRP-conjugated goat anti-mouse secondary antibody	Proteintech Group, Inc.	SA00001-1	1:10,000

Table VI. Probes for RNA pull-down assay.

Primer name	Sequences
probe NC forward primers	GAATACTACGCATGCCTACCGATCCGTTCGTCGCGTCAGCAATAATTTAA GCTAATCGCTAATGCAGCGTATATACGTATC
probe NC reverse primers	GATACGTATATACGCTGCATTAGCGATTAGCTTAAATTATTGCTGACGCG ACGAACGGATCGGTAGGCATGCGTAGTATTC
probe circRAD18 forward primers	GAATCTTGCTGTCAAAGTATATACTCCTGTAGCCTCCAGACAGTCTTTAA AGCAGGGGAGCAGGTTAATGGATAATTTCT
probe circRAD18 reverse primers	AGAAATTATCCATTAACCTGCTCCCCTGCTTTAAAGACTGTCTGGAGGCT ACAGGAGTATATACTTTGACAGCAAGATTC

NC, negative control; circ, circular RNAs.

at 4˚C. For each reaction, 100 μl cell lysate was mixed with 200 μl RIP washing buffer and 10 μg probe. The circRAD18 and control probes were incubated alongside the cell lysate overnight at 4˚C. To create circRNA-probe-bead complexes, 50 μl pre-washed magnetic bead suspension was incubated with 300 μl probe-complex solution for 1 h at room temperature after hybridization. After bead incubation, the samples were briefly centrifuged at 61 x g for 1 min and the complexes were then washed six times with RIP washing buffer. Purified RNA attached to the beads was evaluated by RT-qPCR following bead washing using a washing buffer. Table VI lists the probe sequences.

Nude mouse subcutaneous xenograft tumor models. A total of 18 six-week-old male BALB/c nude mice (body weight 18-20 g) were obtained from Hunan SJA Laboratory Animal Co., Ltd. Mice were housed in a specific pathogen-free animal facility using individually ventilated cages supplied by Suzhou Fengshi Experimental Animal Equipment Co., Ltd. The housing conditions were maintained at a controlled temperature of 21.0-25.0˚C and relative humidity of 40-70%, under a 12-h light/dark cycle with an air exchange rate of ≥15 times per h. Mice had *ad libitum* access to standard laboratory chow (Wuhan Wanqian Jiaxing Biotechnology Co., Ltd.) and sterilized purified water. U87 cells were divided into three groups. After lentiviral infection, nude mice's axillae were subcutaneously injected with sh-circRAD18-NC, sh1-circRAD18 and sh2-circRAD18 cells. Once tumors had formed, tumor volume was recorded every 3 days and growth curves were plotted. After 4 weeks, mice were euthanized by intraperitoneal injection of 1.25% tribromoethanol at a dose of 250 mg/kg, followed by cervical dislocation after confirmation of deep anesthesia. Tumors were then excised and weighed. Tumor volume was calculated using the formula: volume=0.5x length x width^2. Animal experiments were performed according to the principles and procedures approved by the Animal Experimentation Ethics Committee of Affiliated Hospital of North Sichuan Medical College (approval no. 202410171).

Immunohistochemistry (IHC). Dehydration of the tissue samples was achieved using a graded ethanol series (China National Pharmaceutical Group Corporation), followed by clearing with xylene (China National Pharmaceutical Group Corporation) and embedding in paraffin (China National Pharmaceutical Group Corporation) at 60˚C. Tissue sections were cut at 3 μm using a microtome (Leica Microsystems GmbH), placed on slides and allowed to dry for 3 h at 60˚C.

Following xylene deparaffinization, graded ethanol was used to rehydrate the slides and distilled water was used to rinse them. 0.01 M Tris-EDTA [pH 9.0; Keycell Biotech (Wuhan) Co., Ltd.] was used for antigen retrieval on a hot plate for 15 min, followed by cooling to room temperature. Endogenous peroxidase activity was blocked with 3% hydrogen peroxide (China National Pharmaceutical Group Corporation) for 15 min at room temperature, then incubated with normal goat serum (Wuhan Boster Biological Technology, Ltd.) for 30 min at room temperature. The sections were incubated overnight at 4˚C with rabbit polyclonal anti-LUC7L2 antibody (Novus Biologicals; cat. no. NBP2-33621; dilution, 1:200). Following a wash, the sections were incubated with an HRP-labeled goat anti-rabbit/mouse secondary antibody provided in an immunohistochemical detection kit (Dako; Agilent Technologies, Inc.; cat. no. K5007) for 30 min at 37˚C. DAB chromogen from the same kit was used for signal detection, and the reaction was stopped using deionized water. Mayer's hematoxylin [Keycell Biotech (Wuhan) Co., Ltd.] was used to counterstain the sections for 2 min at room temperature, after which they were dehydrated, cleared and mounted using neutral resin. Slides were imaged using an Olympus BX53 light microscope (Olympus Corporation) at magnifications of x100 and x400.

Isolation of exosomes. Ultracentrifugation was used to isolate the exosomes from the cell culture medium. Cell debris was removed using centrifugation at 400 x g for 15 min at 4˚C. The supernatant was then collected using centrifugation at 10,000 x g for 30 min at 4˚C. After obtaining the supernatant, it was ultracentrifuged once again for 70 min at 100,000 x g at 4˚C. The exosomes were rinsed in PBS and ultracentrifuged at 100,000 x g for 70 min at 4˚C after the top layer (supernatant) was removed. 100 μl PBS was used to resuspend the exosomes. Western blotting was used to validate exosome identification by detecting the exosome markers CD9 and CD63.

Transmission electron microscopy (TEM). Copper grids were plasma-cleaned for 10-30 sec with the carbon-coated side facing up. Sealing film was placed on an ice-cold plate to cool. Grids were transferred onto the chilled sealing film, followed by sequential addition of 20 μl drops of the sample, ultrapure water and phosphotungstic acid (PTA) solution. After cooling the grids, samples and solutions for 1-2 min, the carbon-coated side was gently placed on the sample droplets for 1 min to allow adsorption. Excess liquid was removed by touching the grid with filter paper until dry, followed by an additional 10 sec of blotting. The grids were then placed on ultrapure water droplets, immediately lifted and blotted dry with filter paper. The grids were stained by placing on PTA droplets for 0.5-1 min, followed by blotting to remove excess PTA. Finally, grids were air-dried in a shaded area and observed using TEM (Tecnai G20 TWIN; FEI; Thermo Fisher Scientific, Inc.).

Nanoparticle tracking analysis (NTA). The NanoSight NS300 (Malvern Instruments, Ltd.) was used to examine the size distribution of exosomes. A camera captured the light scattered by exosomes under laser illumination, producing a video of their Brownian motion. The size of individual particles was tracked and analyzed using NTA software (version 3.3 Dev Build 3.3.104; NanoSight, Malvern Instruments, Ltd.).

Bioinformatics analysis. The Gene Expression Omnibus (GEO) database (https://www.ncbi.nlm.nih.gov/geo/) provides information on the expression of circRNAs, miRNAs and mRNAs in GBM. The exoRBase database (http://www.exorbase.org:9000/) provides access to circRNA data from exosome-derived GBM cells. The Chinese Glioma Genome Atlas (CGGA) database (http://www.cgga.org.cn) provides clinical information, WHO grades and expression data for miR-1231 and LUC7L2, rated from low to high. The possible target miRNAs of circRAD18 were then predicted using the CircBank (http://www.CircBank.cn/) and CircInteractome (http://circinteractome.nia.nih.gov/) databases. Utilizing the TargetScan database (https://www.targetscan.org/), the mirDIP database (https://ophid.utoronto.ca/mirDIP/index_confirm.jsp) and the miRwalk database (http://mirwalk.umm.uni-heidelberg.de/), possible miR-1231 target mRNAs were predicted.

Statistical analysis. Statistical analysis was conducted using SPSS Statistics software (version 25.0; IBM Corp.). Statistical significance between groups was assessed using the t-test, Mann-Whitney U test, or one-way analysis of variance (ANOVA) followed by Bonferroni's post hoc test, as appropriate. Survival rates were analyzed using the Kaplan-Meier method. Results are presented as mean ± standard error of the mean (SEM). $P<0.05$ was considered to indicate a statistically significant difference.

Results

circRAD18 exhibits high expression in both GBM cell lines and tissues. The GEO database (GSE146463; https://www.ncbi.nlm.nih.gov/geo/query/acc.cgi?acc=GSE146463) was initially screened to investigate the difference in circRNA expression between GBM cells and NBTs. A fold change of >1 and a $P<0.05$ were used as screening criteria and it was found that 1,965 circRNAs were substantially expressed in GBM (Fig. 1A and B). Subsequently, the exoRBase database was searched and 511 circRNAs expressed in GBM-derived exosomes identified. In parallel, a total of 1,965 circRNAs were identified from GSE146463. Among them, 45 circRNAs were shared between the two datasets, whereas 1,920 and 466 circRNAs were specific to GSE146463 and exoRBase, respectively (Fig. 1C). Among the 45 circRNAs overlapping between GSE146463 and exoRBase, circRAD18 was selected for further investigation because it exhibited relatively high expression in GBM-derived exosomes compared with other tumor types (Fig. 1D). According to the circBase database, circRAD18 is derived from the RAD18 gene, with its splicing structure depicted in Fig. 1E. As circRNAs are resistant to RNase R digestion, RNase R treatment experiments were performed. The findings showed that whereas circRAD18 expression was mostly unaltered after RNase R treatment, linear RAD18 mRNA expression was markedly decreased (Fig. 1F). The effective amplification of circRAD18 from cDNA using divergent primers and its resistance to RNase R treatment were verified by RT-qPCR and agarose gel electrophoresis (Fig. 1G). These findings confirmed that circRAD18 adopts a circular structure. Furthermore, circRAD18 was found to be notably more abundant in GBM cell lines and

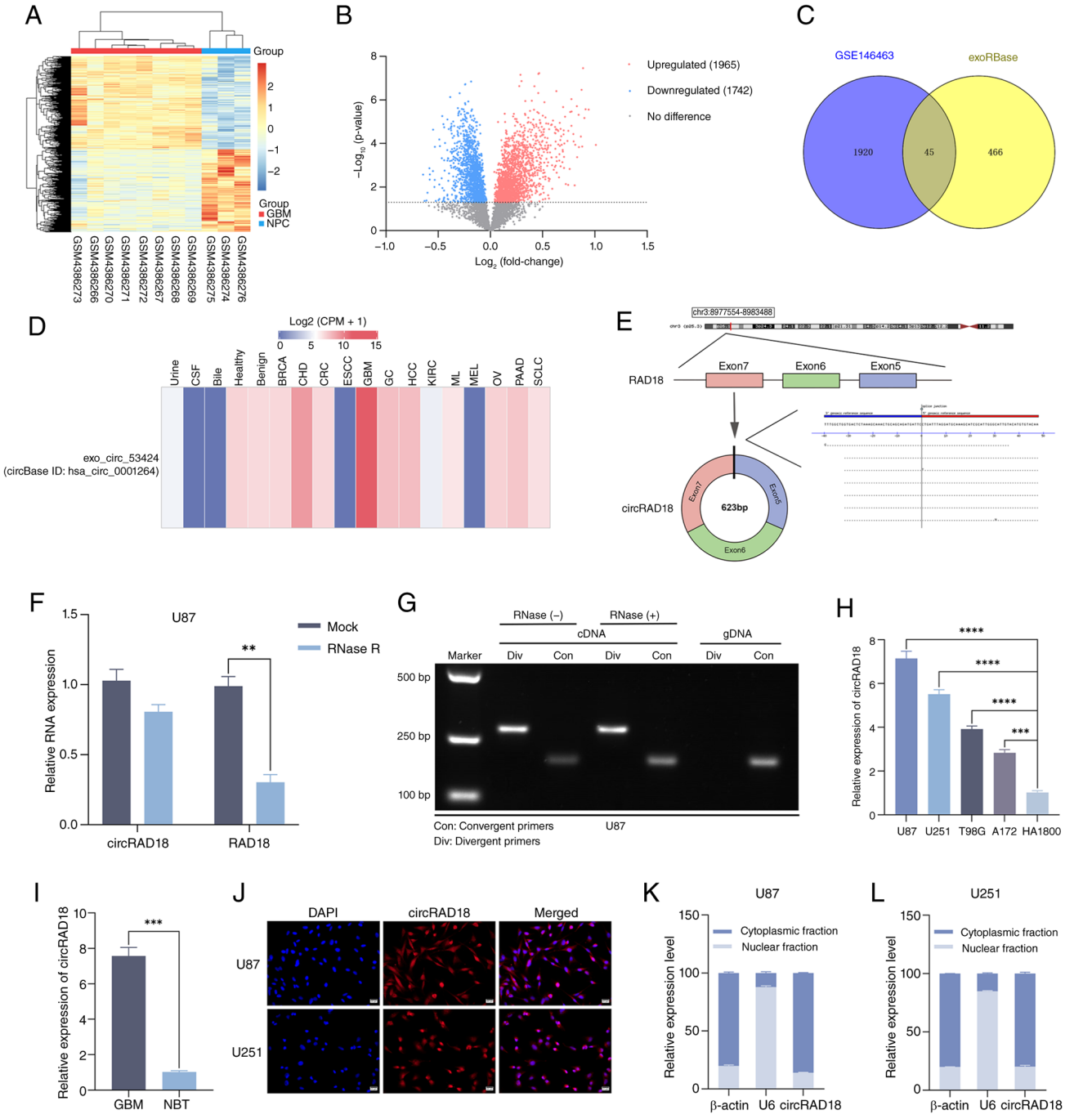

Figure 1. circRAD18 is highly expressed in GBM cell lines and tissues. (A) Heatmap showing hierarchical clustering of 3707 differentially expressed circRNAs between GBM cells and NPCs. (B) Volcano plot showing differentially expressed circRNAs in GBM cells, with 1,965 upregulated and 1,742 downregulated. (C) Venn diagram demonstrating that 45 circRNAs expressed in GBM-derived exosomes overlapped with the 1965 upregulated circRNAs in GBM cells. (D) circRAD18 expression was markedly upregulated in GBM cell-derived exosomes, as identified in the exoRBase database. (E) Schematic representation of the genomic location, circular structure exon composition and back-splice junction of circRAD18. (F) RNase R treatment showing that circRAD18 was resistant to digestion, confirming its circular stability. (G) RT-qPCR products amplified with divergent and convergent primers were analyzed by agarose gel electrophoresis, confirming the circular form of circRAD18. (H) RT-qPCR showed that circRAD18 expression was markedly higher in GBM cell lines than in normal astrocytes. (I) RT-qPCR showing that circRAD18 expression was markedly higher in GBM tissues (n=74) than in adjacent normal brain tissues (n=21). (J) FISH was used to detect the localization of circRAD18 in the cytoplasm. Red denotes circRAD18, while blue shows nuclei stained with DAPI. Scale bar, 20 μm. Subcellular localization of circRAD18 in (K) U87 and (L) U251 cells was determined by nuclear and cytoplasmic fractionation followed by RT-qPCR. β-actin and U6 were used as cytoplasmic and nuclear markers, respectively. circRAD18 was predominantly localized in the cytoplasmic fraction. All data are presented as mean ± SEM and each experiment was performed in triplicate. **P<0.01; ***P<0.001; ****P<0.0001. circ, circular RNA; GBM, glioblastoma; NPCs, neural progenitor cells; RT-qPCR, reverse transcription-quantitative PCR; FISH, fluorescence *in situ* hybridization.

tissues than in normal astrocyte HA1800 cells and NBTs (Fig. 1H and I). U87 and U251 cell lines, which exhibited the highest circRAD18 expression, were selected for subsequent experiments. Since the intracellular location of circRNAs is frequently associated with their function, FISH experiments combined with cytoplasmic/nuclear fractionation analyses showed that circRAD18 was predominantly located in the cytoplasm (Fig. 1J-L).

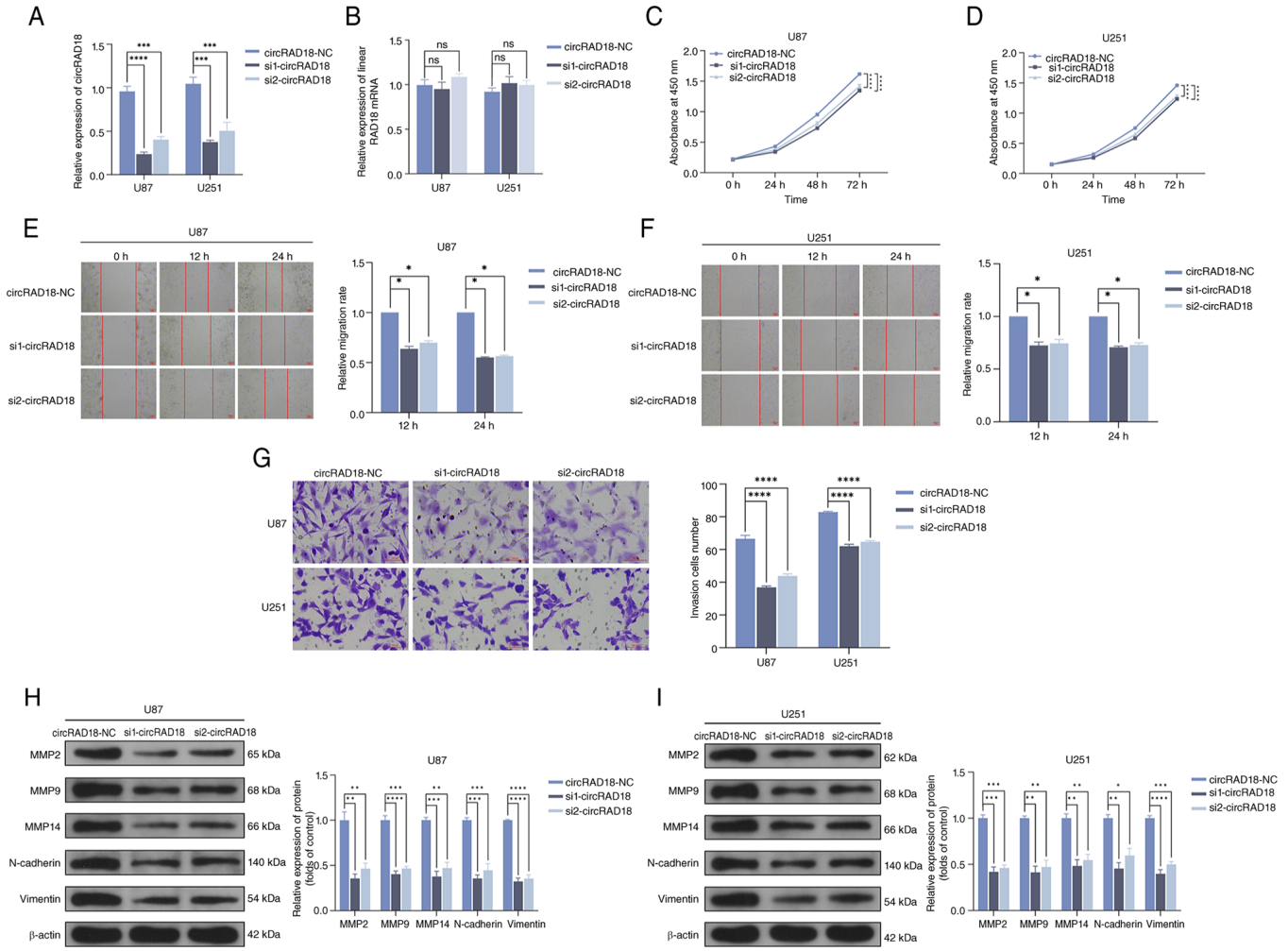

Figure 2. circRAD18 knockdown suppresses GBM cell proliferation, migration and invasion *in vitro*. (A) RT-qPCR analysis showing that circRAD18 expression was markedly reduced in U87 and U251 cells after siRNA transfection. (B) RT-qPCR analysis showing that siRNA transfection did not affect the expression levels of linear RAD18 mRNA. CCK-8 assays showing that circRAD18 knockdown markedly inhibited the proliferation of (C) U87 and (D) U251 cells. Wound healing assays showing that circRAD18 knockdown markedly reduced the migration of (E) U87 and (F) U251 cells. Scale bar, 100 μm. (G) Transwell assays showing that circRAD18 knockdown markedly inhibited the invasion of U87 and U251 cells. Scale bar, 100 μm. Western blot analysis showing that circRAD18 knockdown reduced the expression of invasion-related proteins MMP2, MMP9, MMP14, N-cadherin and Vimentin in (H) U87 and (I) U251 cells. All data are presented as mean ± SEM and each experiment was performed in triplicate. *P<0.05; **P<0.01; ***P<0.001; ****P<0.0001. circ, circular RNA; GBM, glioblastoma; RT-qPCR, reverse transcription-quantitative PCR; si, small interfering.

circRAD18 knockdown inhibits GBM cell proliferation, migration and invasion. A total of two siRNAs that target circRAD18 were created and transfected into GBM cells to examine the function of circRAD18 in the development of GBM. RT-qPCR results confirmed that these two siRNAs effectively reduced circRAD18 expression (Fig. 2A) without affecting linear RAD18 mRNA levels (Fig. 2B). As demonstrated by CCK-8 assays, circRAD18 knockdown markedly reduced GBM cell proliferation (Fig. 2C and D). GBM cell migration was markedly impaired by circRAD18 knockdown, as shown by wound healing assays (Fig. 2E and F). Additionally, Transwell assays showed that knocking down circRAD18 reduced the invasive capacity of GBM cells (Fig. 2G). Furthermore, circRAD18 knockdown markedly decreased the amounts of invasion-related proteins in GBM cells, including MMP2, MMP9, MMP14, N-cadherin and vimentin, according to western blot analysis (Fig. 2H and I). According to the findings, circRAD18 contributes to GBM cell invasion, migration and proliferation.

circRAD18 acts as a sponge for miR-1231. Prior research has demonstrated that circRNAs primarily control gene expression by serving as miRNA sponges. Bioinformatic analysis via CircBank and CircInteractome databases was used to identify miRNA targets of circRAD18, selecting miR-1231, miR-1248, miR-556-5p and miR-626 for further validation (Fig. 3A). The analysis of the GEO database (GSE90603) identified 807 miRNAs with downregulated expression (fold change <1; P<0.05) in GBM cells (Fig. 3B), including miR-1231 (Fig. 3C). Additionally, research by Zhang *et al* (27) and Wang *et al* (28) showed that GBM is associated with underexpression of miR-1231. CGGA database data indicated that lower miR-1231 expression correlates with increased glioma malignancy, with lower miR-1231 levels corresponding to higher WHO grades (Fig. 3D). Additionally, patients with higher miR-1231 expression exhibited longer survival times (Fig. 3E). FISH experiments and cytoplasmic/nuclear fractionation analyses revealed that circRAD18 co-localizes with miR-1231 in the cytoplasm (Fig. 3F-H). miR-1231 mimics or

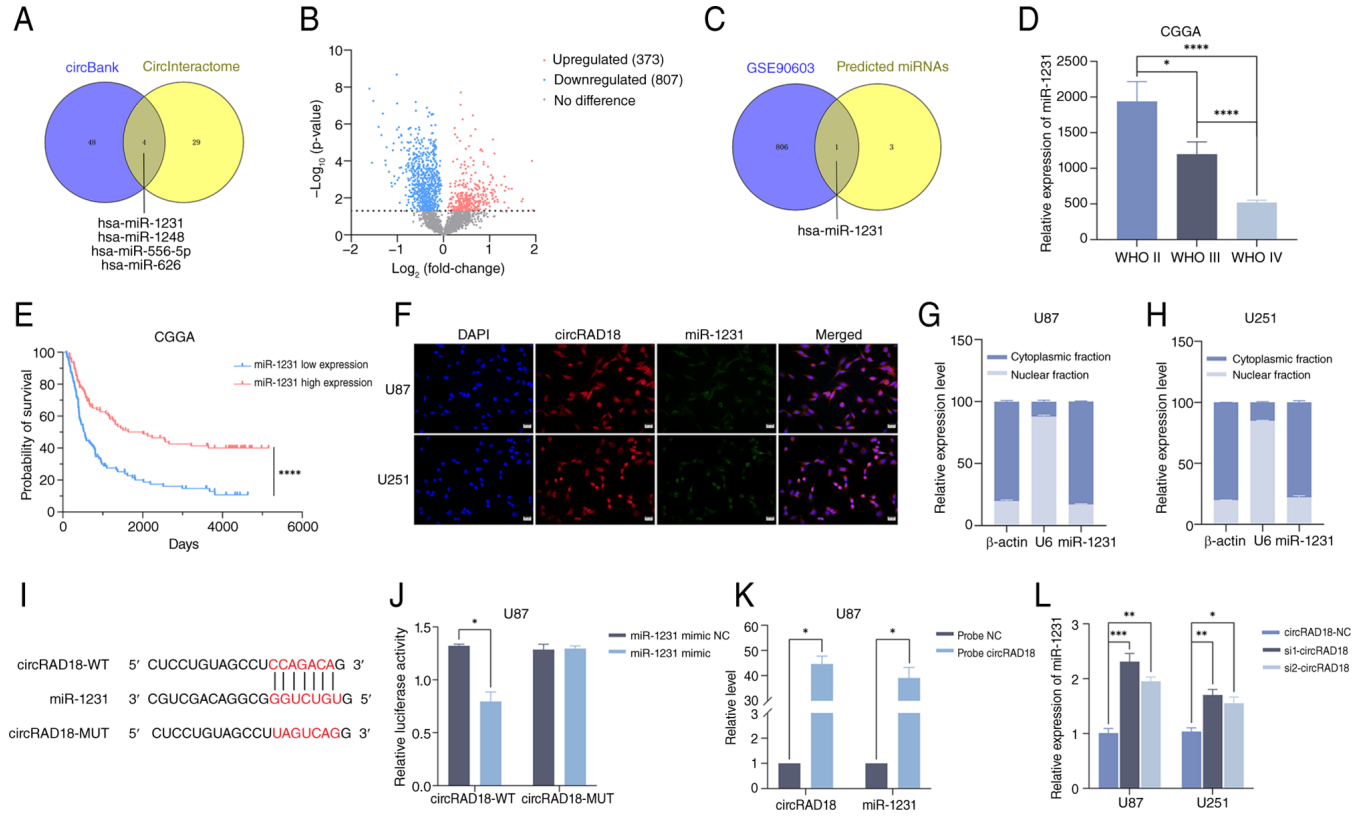

Figure 3. CircRAD18 acts as a sponge for miR-1231 in GBM cells. (A) Venn diagram showing miRNA targets of circRAD18 predicted using the CircBank and CircInteractome databases. (B) Volcano plot showing differentially expressed miRNAs in GBM cells, including 373 upregulated and 807 downregulated. (C) Venn diagram illustrating the overlap between predicted miRNAs and downregulated miRNAs from the GSE90603 dataset. (D) Data from the CGGA database showing that miR-1231 expression decreased as glioma grade increased. (E) Using data from the CGGA database, patients were categorized by miR-1231 levels and generated Kaplan-Meier survival curves to compare survival rates between the two groups. (F) FISH was used to detect the co-localization of circRAD18 and miR-1231 in the cytoplasm of GBM cells. circRAD18 is shown in red, miR-1231 in green, and nuclei are stained blue with DAPI. Scale bar, 20 μm. Nucleocytoplasmic fractionation analysis followed by RT-qPCR demonstrated that miR-1231 was predominantly localized in the cytoplasm of (G) U87 and (H) U251 cells. β-actin and U6 were used as cytoplasmic and nuclear markers, respectively, to validate the fractionation efficiency. (I) Predicted binding sites of miR-1231 in circRAD18, with the Mut version of circRAD18 presented. (J) The dual-luciferase reporter assay determining the binding between circRAD18 and miR-1231. (K) RNA pull-down assay performed to verify the direct binding between circRAD18 and miR-1231. (L) RT-qPCR showed that circRAD18 knockdown markedly increased miR-1231 expression in U87 and U251 cells. All data are presented as mean ± SEM and each experiment was performed in triplicate. *P<0.05; **P<0.01; ***P<0.001; ****P<0.0001. circ, circular RNA; GBM, glioblastoma; miRNA, microRNA; CGGA, Chinese Glioma Genome Atlas; FISH, fluorescence *in situ* hybridization; RT-qPCR, reverse transcription-quantitative PCR; MUT, mutant; WT, wild type.

a control were co-transfected into U87 cells using wild-type and mutant luciferase reporter vectors to confirm the binding location of circRAD18 with miR-1231. The outcomes demonstrated that cells transfected with a wild-type vector and treated with miR-1231 mimics exhibited a substantial decrease in luciferase activity, but cells transfected with a mutant vector did not exhibit this effect (Fig. 3I and J). Using a biotin-labeled circRAD18 probe, RNA pull-down experiments were performed in U87 cells to verify direct interaction between circRAD18 and miR-1231. Compared with the control oligonucleotide probe, the circRAD18 probe markedly increased pull-down efficiency and enriched miR-1231 (Fig. 3K). Subsequently, we examined miR-1231 expression after circRAD18 knockdown and found that miR-1231 was upregulated (Fig. 3L). These results suggest that circRAD18 interacts with miR-1231, playing a regulatory role in the process.

miR-1231 directly targets LUC7L2. To identify the molecular targets of miR-1231, the TargetScan, miRDIP and miRWalk databases were used to predict 61 downstream targets (Fig. 4A). The GEO database (GSE4290) was then searched and 2,499 highly expressed mRNAs in GBM cells identified (fold change >1; P<0.05; (Fig. 4B), with 9 mRNAs overlapping the 61 predicted targets (Fig. 4C). The expression of these nine mRNAs across glioma grades was analyzed using the CGGA database and it was discovered that LUC7L2 expression was noticeably greater in high-grade gliomas than in low-grade gliomas (Fig. 4D), whereas the other candidate genes displayed lower expression levels or lacked a clear association with tumor grade (Fig. S1). Higher LUC7L2 expression was also associated with poorer survival outcomes (Fig. 4E). Studies have shown that miRNAs regulate target mRNAs by inhibiting transcription or inducing degradation through binding to the 3'-UTR (29-31). It was hypothesized that miR-1231 interacts with the 3'UTR of LUC7L2 mRNA to control GBM development. A dual-luciferase reporter experiment was employed to confirm that miR-1231 binds to LUC7L2. U87MG cells were co-transfected with either wild-type or mutant LUC7L2 3'-UTR plasmids and miR-1231 mimics. Luciferase activity was considerably decreased by co-transfection with the wild-type plasmid and miR-1231 mimics (Fig. 4F and G).

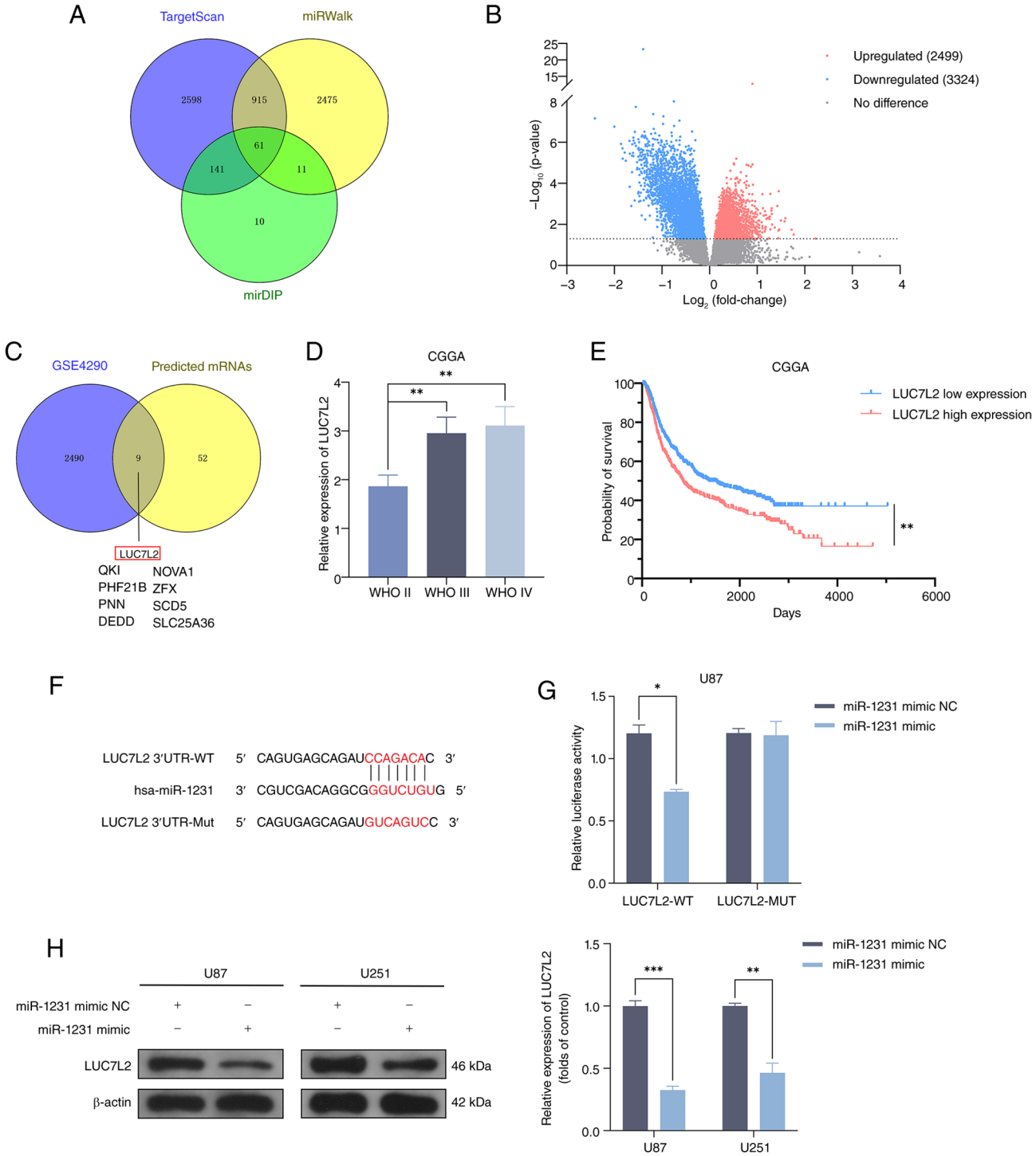

Figure 4. miR-1231 directly targets LUC7L2. (A) Venn diagram showing predicted miR-1231 target mRNAs using TargetScan, miRWalk and mirDIP databases. (B) Volcano plot showing differentially expressed mRNAs in GBM cells, with 2,499 upregulated and 3,324 downregulated. (C) Venn diagram illustrating the overlap between predicted mRNAs and upregulated mRNAs from the GSE4290 dataset. (D) Data from the CGGA database indicating that LUC7L2 expression increased with glioma grade. (E) Using data from the CGGA database, patients were categorized by LUC7L2 levels and generated Kaplan-Meier survival curves to compare the survival rates between the two groups. (F) Predicted binding sites of miR-1231 in LUC7L2 3'-UTR, with the Mut version of LUC7L2 3'-UTR presented. (G) The dual-luciferase reporter assay confirming the binding between miR-1231 and LUC7L2. (H) Western blot analysis showing that miR-1231 mimic treatment reduced LUC7L2 protein levels in U87 and U251 cells. All data are presented as mean ± SEM and each experiment was performed in triplicate. *P<0.05; **P<0.01; ***P<0.001. miRNA, microRNA; GBM, glioblastoma; CGGA, Chinese Glioma Genome Atlas; NC, negative control; MUT, mutant; WT, wild type.

Furthermore, transfection of miR-1231 mimics was found to decrease LUC7L2 protein levels substantially (Fig. 4H). These results implied that miR-1231 directly targets the gene LUC7L2.

circRAD18 regulates GBM cell proliferation, migration and invasion in association with the miR-1231/LUC7L2 axis. The present study performed a series of experiments in U87 and U251 cells to explore whether circRAD18 is involved in GBM

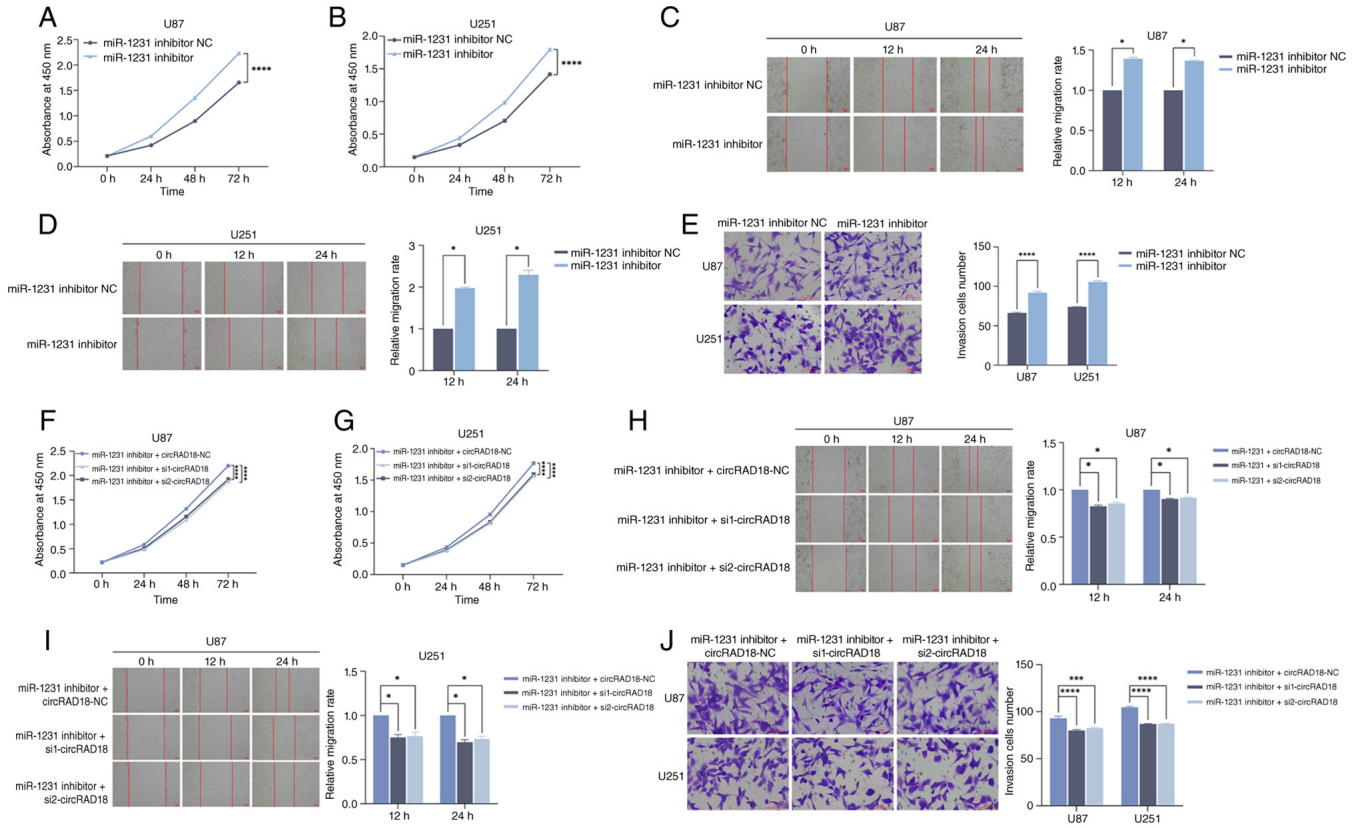

Figure 5. circRAD18 promotes the proliferation, migration and invasion of GBM cells by sponging miR-1231. CCK-8 assays showing that miR-1231 inhibitor transfection promoted the proliferation of (A) U87 and (B) U251 cells. Wound healing assays showing that miR-1231 inhibitor transfection enhanced the migration of (C) U87 and (D) U251 cells. Scale bar, 100 μm. (E) Transwell assays showed that miR-1231 inhibitor transfection promoted the invasion of U87 and U251 cells. Scale bar, 100 μm. CCK-8 assays showing that si-circRAD18 co-transfection attenuated the proliferation-promoting effect of miR-1231 inhibitor in (F) U87 and (G) U251 cells. Wound healing assays showing that si-circRAD18 co-transfection attenuated the migration-promoting effect of miR-1231 inhibitor in (H) U87 and (I) U251 cells. Scale bar, 100 μm. (J) Transwell assays showing that si-circRAD18 co-transfection attenuated the invasion-promoting effect of miR-1231 inhibitor in U87 and U251 cells. Scale bar, 100 μm. All data are presented as mean ± SEM and each experiment was performed in triplicate. *P<0.05; ***P<0.001; ****P<0.0001. circ, circular RNA; GBM, glioblastoma; miRNA, microRNA; si, small interfering.

progression in association with the miR-1231/LUC7L2 axis. Using CCK-8, wound healing and Transwell assays, it was observed that miR-1231 inhibitor transfection enhanced GBM cell proliferation, migration and invasion (Fig. 5A-E), while knockdown of circRAD18 attenuated these effects (Fig. 5F-J). Western blot analysis revealed that LUC7L2 protein levels were notably reduced by circRAD18 knockdown (Fig. 6A). Transfection of miR-1231 inhibitor markedly increased LUC7L2 protein levels (Fig. 6B), while co-knockdown of circRAD18 partially reversed this effect in GBM cells (Fig. 6C). Furthermore, to evaluate the downstream role of LUC7L2, LUC7L2-overexpressing cell models were established (Fig. 6D-E). Overexpression of LUC7L2 promoted GBM cell proliferation, migration and invasion as assessed by CCK-8, wound healing and Transwell assays (Fig. 6F-J) and knockdown of circRAD18 partially attenuated these effects (Fig. 6K-O). Collectively, these experiments supported the involvement of a circRAD18/miR-1231/LUC7L2 regulatory axis in GBM cell proliferation, migration and invasion.

circRAD18 downregulation inhibits GBM cell growth in vivo. The U87 cell line was split into three groups: A NC group and two shRNA knockdown groups that targeted circRAD18 (sh1-circRAD18 and sh2-circRAD18) to assess the effect of circRAD18 on GBM cell growth *in vivo*. Then, cells were subcutaneously injected into the axillae of BALB/c nude mice to establish xenograft tumor models. The xenograft models exhibited a notable decrease in tumor growth rate, volume and weight in the circRAD18 knockdown group (Fig. 7A-E). RT-qPCR analysis revealed that in the circRAD18 knockdown group, circRAD18 expression decreased (Fig. 7F), miR-1231 expression increased (Fig. 7G) and LUC7L2 mRNA expression decreased (Fig. 7H) compared with the control group. LUC7L2 expression was much lower in the circRAD18 knockdown group, according to IHC (Fig. 7I). These findings suggested that circRAD18 facilitates malignant GBM cell development *in vivo*.

circRAD18 is enriched in GBM cell-derived exosomes. By searching the exoRBase database, high expression of circRAD18 was identified in exosomes derived from GBM cells. Next, the EVs were isolated from the culture supernatant of the HA1800 normal astrocytes and the U87 cells. TEM and NTA showed that the EVs were round, had a bilayer membrane and ranged in size from 50-120 nm (Fig. 8A and B). The exosomal markers CD63 and CD9 were shown to be positively expressed in the isolated EVs by western blot analysis (Fig. 8C). These findings indicated successful isolation of exosomes. circRAD18 expression was substantially greater in exosomes obtained from U87 cells than in exosomes derived from HA1800 cells, according to RT-qPCR analysis (Fig. 8D).

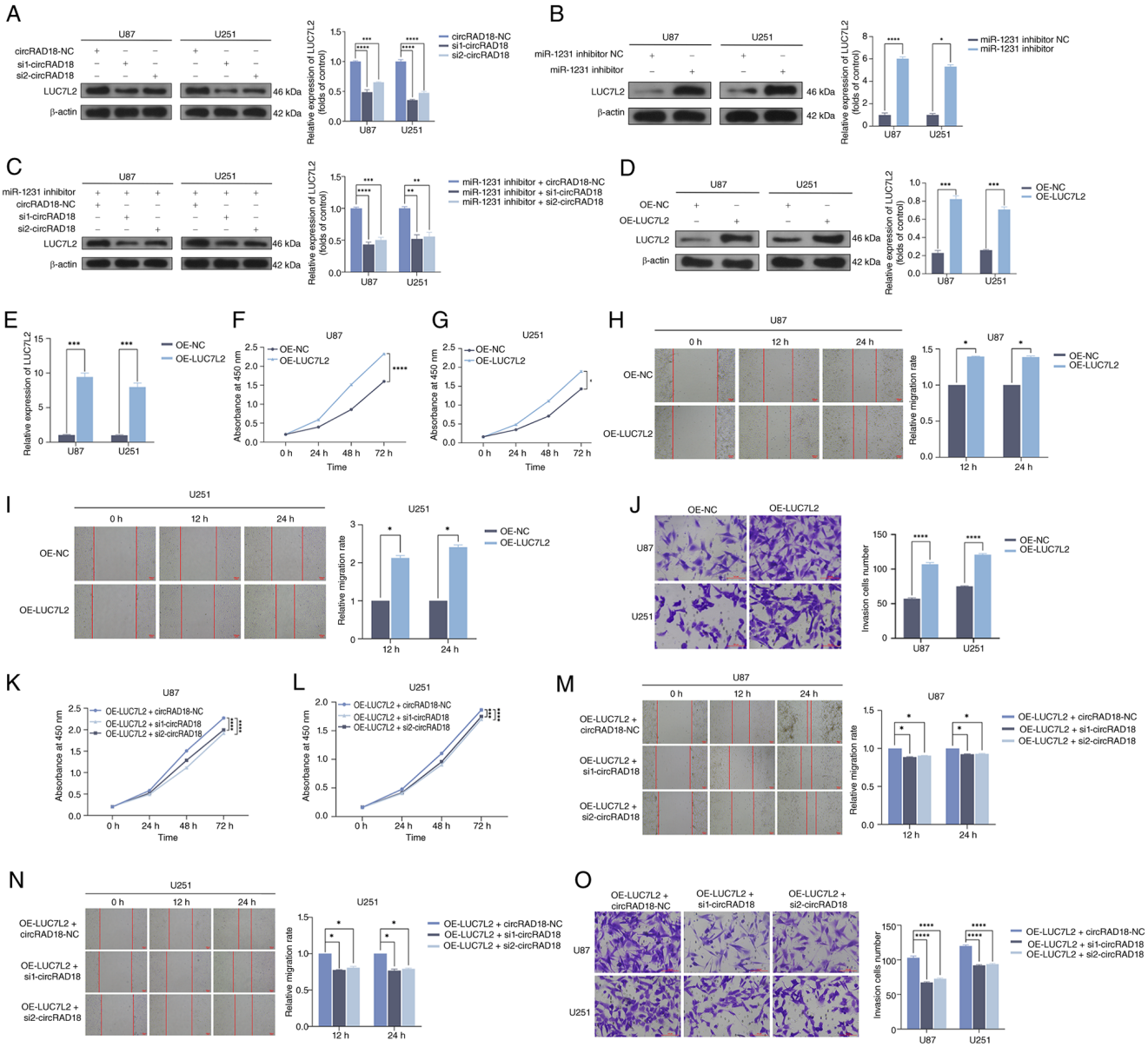

Figure 6. circRAD18 promotes the proliferation, migration and invasion of GBM cells through the miR-1231/LUC7L2 axis. (A) Western blot analysis showing that circRAD18 knockdown reduced LUC7L2 protein levels in U87 and U251 cells. (B) Western blot analysis showing that miR-1231 inhibitor increased LUC7L2 protein levels in U87 and U251 cells. (C) Western blot analysis showing that si-circRAD18 co-transfection attenuated the increase in LUC7L2 protein levels induced by miR-1231 inhibitor in U87 and U251 cells. (D) Western blot analysis showing that LUC7L2 overexpression increased LUC7L2 protein levels in U87 and U251 cells. (E) RT-qPCR analysis showing that LUC7L2 overexpression increased LUC7L2 expression in U87 and U251 cells. CCK-8 assays showing that LUC7L2 overexpression promoted the proliferation of (F) U87 and (G) U251 cells. Wound healing assays showing that LUC7L2 overexpression enhanced the migration of (H) U87 and (I) U251 cells. Scale bar, 100 μm. (J) Transwell assays showing that LUC7L2 overexpression promoted the invasion of U87 and U251 cells. Scale bar, 100 μm. CCK-8 assays showing that circRAD18 knockdown attenuated the proliferation-promoting effect of LUC7L2 overexpression in (K) U87 and (L) U251 cells. Wound healing assays showing that circRAD18 knockdown attenuated the migration-promoting effect of LUC7L2 overexpression in (M) U87 and (N) U251 cells. Scale bar, 100 μm. (O) Transwell assays showed that circRAD18 knockdown attenuated the invasion-promoting effect of LUC7L2 overexpression in U87 and U251 cells. Scale bar, 100 μm. All data are presented as mean ± SEM and each experiment was performed in triplicate. *P<0.05; **P<0.01; ***P<0.001; ****P<0.0001. circ, circular RNA; GBM, glioblastoma; miRNA, microRNA; si, small interfering; RT-qPCR, reverse transcription-quantitative PCR; OE, overexpressed; NC, negative control.

Based on these results, exosomal circRAD18 could potentially serve as a biomarker for GBM.

Discussion

As the most prevalent and lethal type of glioma (32,33), GBM is challenging to treat because total surgical resection is difficult to achieve and GBM has high resistance to chemotherapy and radiation (34,35). Its rapid proliferation, along with strong migratory and invasive capacities, leads to high recurrence and mortality rates (36,37). Thus, there is an urgent need to identify novel treatment targets for GBM. circRNAs represent a novel class of ncRNAs. circRNAs have been implicated in critical physiological processes, including angiogenesis (38,39), autophagy (40,41) and apoptosis (42,43) in recent investigations. Additionally, circRNAs have been shown to have oncogenic or tumor-suppressive functions in several malignancies, including bladder, breast, pancreatic

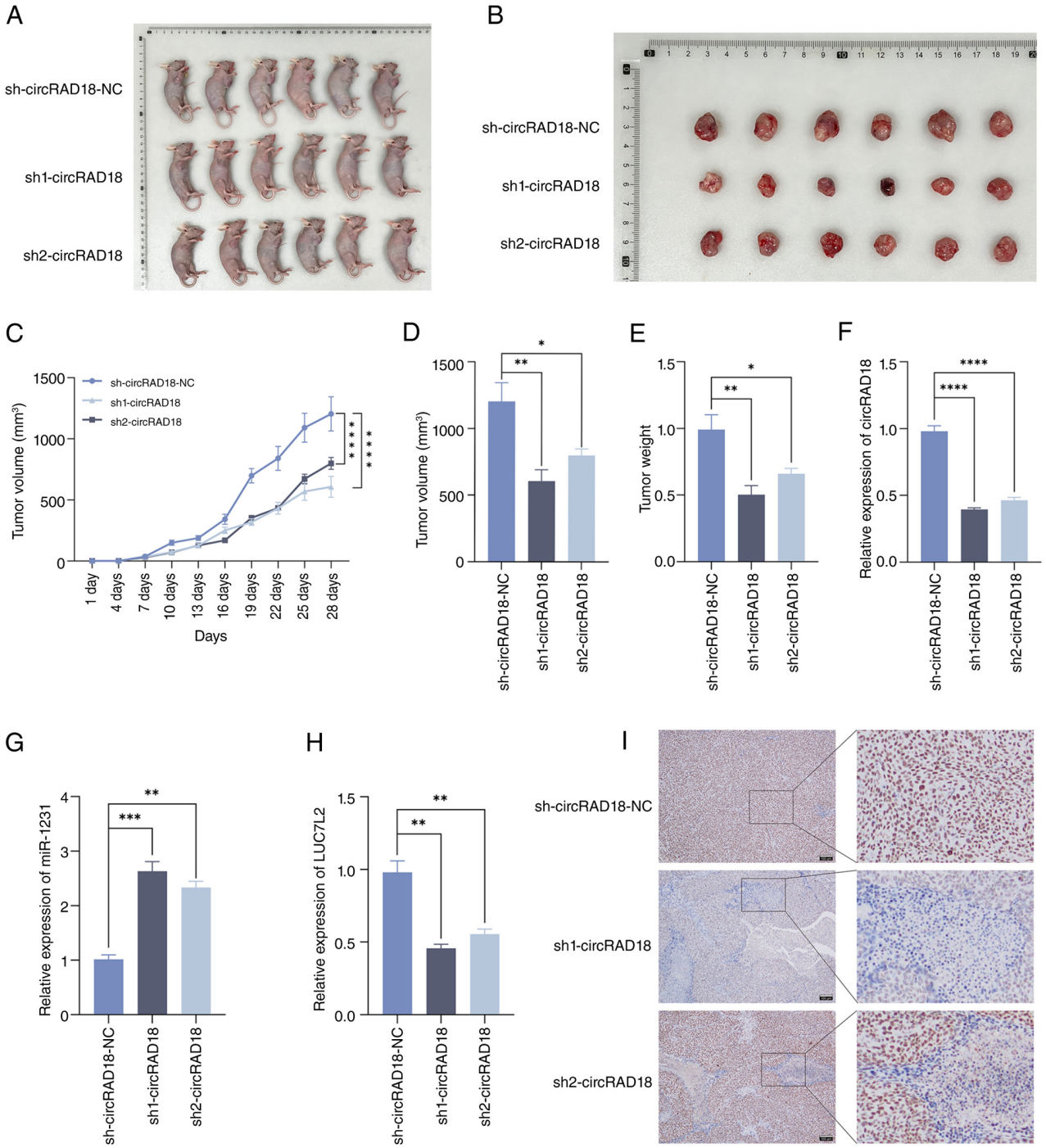

Figure 7. circRAD18 knockdown inhibits GBM progression *in vivo*. (A and B) Representative images of xenograft tumors in nude mice showing that circRAD18 knockdown reduced tumor growth. (C) Tumor growth curves showing that circRAD18 knockdown slowed the growth of subcutaneous xenograft tumors. (D) Tumor volume measurements at day 28 showing that circRAD18 knockdown reduced tumor size compared with the control group. (E) Tumor weights measured on day 28 showing that circRAD18 knockdown decreased tumor mass compared with the control group. (F) RT-qPCR analysis showing that circRAD18 knockdown decreased circRAD18 expression in xenograft tumors. (G) RT-qPCR analysis showing that circRAD18 knockdown increased miR-1231 expression in xenograft tumors. (H) RT-qPCR analysis showing that circRAD18 knockdown decreased LUC7L2 expression in xenograft tumors. (I) IHC staining of xenograft tumors showing that circRAD18 knockdown decreased LUC7L2 protein levels. Scale bar, 100 μm. All data are presented as mean ± SEM and each experiment was performed in triplicate. *P<0.05; **P<0.01; ***P<0.001; ****P<0.0001. circ, circular RNA; GBM, glioblastoma; IHC, immunohistochemistry; RT-qPCR, reverse transcription-quantitative PCR; sh, short hairpin.

and lung cancers (44-47). circRNAs may be involved in brain function and disease, as evidenced by their abundance in brain tissue (14,48). There is evidence that several circRNAs are important for GBM development. For instance, Jiang *et al* (49) revealed that circLRFN5 suppresses GBM progression by promoting ferritin deposition via the PRRX2/GCH1 axis. Long *et al* (50) reported that circPOSTN promotes angiogenesis in GBM by modulating the miR-219a-2-3p/STC1 axis and stimulating vascular endothelial growth factor A (VEGFA) secretion. However, more research is necessary to fully understand the precise roles and regulatory mechanisms of several new circRNAs in GBM.

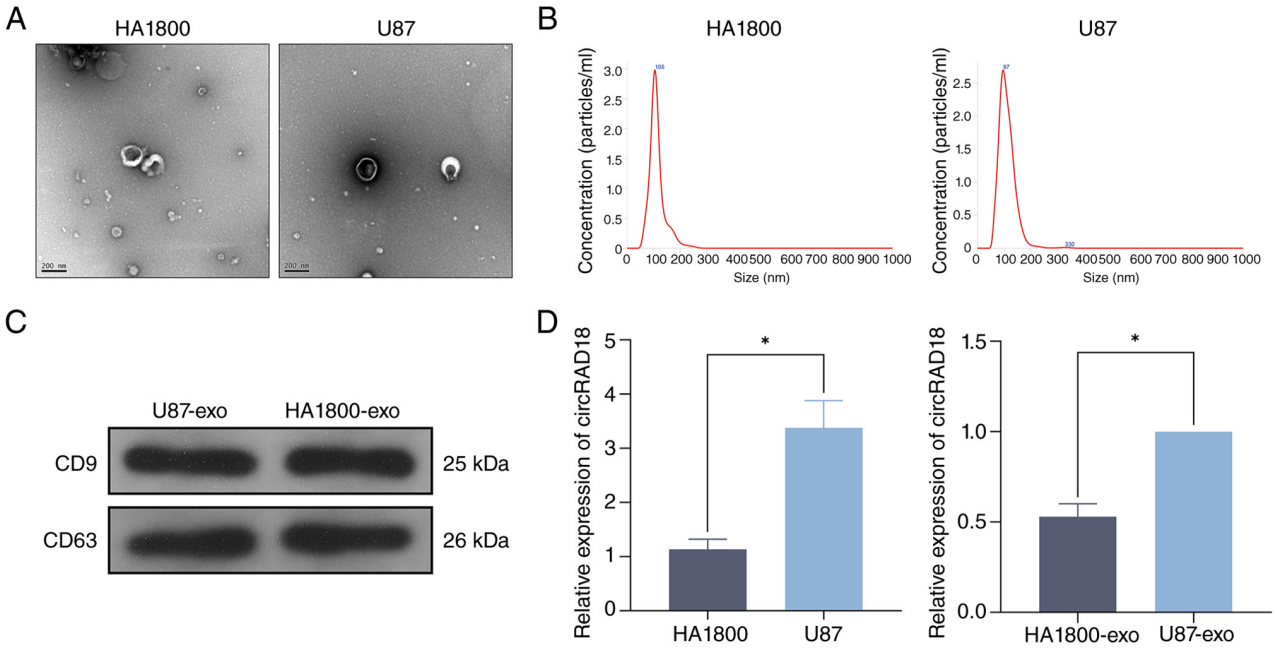

Figure 8. circRAD18 is enriched in GBM cell-derived exosomes. (A) Transmission electron microscopy showing the morphology of exosomes derived from HA1800 and U87 cells. Scale bar, 200 nm. (B) NTA showing that exosomes from HA1800 and U87 cells ranged in size from 50-120 nm. (C) Western blot analysis confirmed the presence of exosomal markers CD9 and CD63 in EVs. (D) The expression of circRAD18 in U87 cells and U87 cell-derived exosomes was markedly higher than in HA1800 cells and HA1800 cell-derived exosomes. All data are presented as mean ± SEM and each experiment was performed in triplicate. *P<0.05. circ, circular RNA; GBM, glioblastoma; IHC, immunohistochemistry; RT-qPCR, reverse transcription-quantitative PCR; NTA, nanoparticle tracking analysis; EVs, extracellular vesicles.

The present study identified circRAD18 through analysis of the GSE146463 microarray data and confirmed its high expression in GBM cells and tissues. This implied that circRAD18 may be employed as a biomarker for GBM diagnosis, prognosis prediction and treatment. Further analysis using the exoRBase database revealed that circRAD18 was abundant in GBM cell-derived exosomes, prompting its selection as the focus of the present study. Previous studies have demonstrated that circRAD18 promotes breast cancer progression (51). To the best of the authors' knowledge, there has never been a report of circRAD18 expression and function in GBM. GBM cell proliferation, migration and invasion were all inhibited by circRAD18 knockdown, as shown by loss-of-function experiments. Further *in vivo* experiments confirmed that circRAD18 suppression inhibited xenograft tumor growth. These results suggested that circRAD18 may play an important role in GBM development and progression, warranting further investigation into its underlying mechanisms.

Studies indicate that most cytoplasmic circRNAs are loaded with miRNA-binding sites, allowing them to act as sponges for miRNAs (3,52,53). Analysis using FISH revealed that circRAD18 was localized in the cytoplasm, leading to the hypothesis that it may function as a miRNA sponge. Bioinformatic analysis indicated that circRAD18 binds to miR-1231. Dual-luciferase reporter and RNA pull-down assays both proved that circRAD18 binds to miR-1231. Prior research has demonstrated the pivotal role of miR-1231 in tumor progression. For example, miR-1231 expression is markedly reduced in small-cell lung cancer, promoting proliferation, migration and invasion of small-cell lung cancer (54). Additionally, Wang *et al* (28) and Zhang *et al* (27) showed that gliomas had downregulated miR-1231, which promotes tumor growth. GEO, TargetScan, miRDIP and miRWalk databases were used to predict the target gene of miR-1231, identifying LUC7L2, which is highly expressed in GBM cells. LUC7L2 is a highly conserved and widely expressed RNA-binding protein (55) and is closely associated with malignant tumor progression. LUC7L2 plays a vital role in myelodysplastic syndrome development (56) while also contributing to radioresistance in nasopharyngeal carcinoma by regulating autophagy (57). According to Yue *et al* (58), the LUC7L2 promoter had substantial enrichment of histone H3K9 lactonization, which activated LUC7L2 transcription. Additionally, LUC7L2 facilitated the retention of MLH1 intron 7, which increased GBM resistance to temozolomide. The present study found that transfection with a miR-1231 inhibitor was associated with increased LUC7L2 expression and enhanced GBM cell proliferation, migration and invasion. By contrast, circRAD18 knockdown inhibited these effects and reduced LUC7L2 expression. GBM cell invasion, migration and proliferation were enhanced by LUC7L2 overexpression, whereas these effects were partially attenuated by circRAD18 knockdown. In conclusion, our findings support the involvement of a circRAD18/miR-1231/LUC7L2 regulatory axis in GBM cell proliferation, migration and invasion.

Studies have demonstrated that exosome-mediated intercellular communication within the tumor microenvironment is vital for tumorigenesis and progression, drawing increased attention to exosomes (59). The bilayer lipid membrane of exosomes protects their bioactive cargo from degradation (60). As natural carriers, exosomes can cross the blood-brain barrier, making them valuable for liquid biopsy and targeted drug delivery. circRNAs, with their circular structure, are stable within cells (61), providing great potential for use in

liquid biopsies for tumor diagnosis (62,63). Consequently, the present study isolated exosomes from HA1800 and U87 cells and discovered that, as verified by RT-qPCR, circRAD18 was markedly increased in exosomes obtained from U87 cells compared with those from HA1800 cells. Based on these results, exosomal circRAD18 may be an insightful biomarker for GBM diagnosis.

However, the present study does have some limitations. First, the clinical sample size was comparatively small, which could potentially lead to selection bias. Further confirmation of the association between circRAD18 and the clinical features of GBM is required. This should be achieved by including a larger patient cohort in future studies. In addition, since the cohort was specifically selected to represent IDH-wildtype GBM in accordance with the 2021 WHO classification, the present study did not compare circRAD18 expression across different molecular subtypes (such as IDH-wildtype vs. IDH-mutant tumors). Future research including diverse molecular subtypes and multi-center data will be essential to elucidate the potential subtype-specific roles of circRAD18. Second, the genotype and phenotype of GBM might not be fully replicated by the GBM cell lines employed in this investigation. Future studies should incorporate a broader range of GBM cell lines or primary cells to improve clinical heterogeneity. Third, there are some limitations in the phenotypic characterization of the present study. While significant changes were observed in mesenchymal markers (N-cadherin and Vimentin) and MMPs, a complete epithelial-to-mesenchymal transition marker panel, including the canonical epithelial marker E-cadherin, was not evaluated. This was partly because the present study primarily focused on the functional aspects of cell invasion, which in the context of GBM-a non-epithelial tumor-are often characterized by the gain of mesenchymal traits. Nevertheless, the absence of E-cadherin data limits the ability to fully assess a balanced phenotypic transition. This is an important point that should be addressed in future studies by incorporating a more comprehensive set of cell adhesion and epithelial markers. From a mechanistic perspective, the current rescue experimental design possessed certain limitations. Although a series of gain- and loss-of-function experiments were performed to examine the circRAD18/miR-1231/LUC7L2 regulatory relationship, this design does not allow for definitive determination of strict directional causality within this axis. In particular, the observed partial rescue effects suggested that circRAD18 may regulate GBM cell proliferation, migration and invasion through additional downstream pathways beyond the miR-1231/LUC7L2 axis. Thus, while the data supported the functional involvement of this regulatory axis, they did not exclude the contribution of other miRNAs or target genes, warranting further investigation using more refined experimental designs. Furthermore, while circRAD18 was detected in GBM-derived exosomes, functional exosome transfer experiments were not conducted in the present study. Consequently, the direct effect of exosomal circRAD18 on recipient cells within the tumor microenvironment was not evaluated and these exosome-mediated intercellular effects require further validation in future investigations. Along the same lines, the downstream signaling pathways by which circRAD18 influences GBM progression, as well as the role of GBM cell-derived exosomal circRAD18 in intercellular communication, require further investigation. Moreover, although the data supported a regulatory interaction whereby circRAD18 acted as a sponge for miR-1231 to influence LUC7L2 expression, deeper mechanistic aspects require clarification, such as whether circRAD18 affects the stability or subcellular localization of miR-1231, or whether other RNA-binding proteins or miRNAs are involved in this regulatory network. Ultimately, the utility of exosomal circRAD18 as a biomarker for GBM diagnosis requires validation using additional clinical samples and functional experiments. Future research will address these questions.

In summary, the present study demonstrated that circRAD18 is markedly upregulated in GBM cells and tissues, functioning as a sponge for miR-1231 to elevate LUC7L2 expression, thereby promoting GBM proliferation, migration and invasion. Moreover, circRAD18 is highly enriched in GBM cell-derived exosomes. These results provided a theoretical foundation for GBM diagnosis, biomarker development and molecular targeted therapies.

Acknowledgements

Not applicable.

Funding

The present study was supported by the Sichuan Medical Science and Technology Innovation Research Association (grant no. YCH-KY-YCZD2024-054), the Health China·BuChang ZhiYuan Public Welfare Projects for Heart and Brain Health of Zhongshe Social Work Development Foundation (grant no. HIGHER2024056), the Affiliated Hospital of North Sichuan Medical College (grant no. 2019ZD001) and the North Sichuan Medical College (grant no. CBY23-ZDA01) and the Bureau of Science and Technology Nanchong City (grant no. 19SXHZ0321).

Availability of data and materials

The data generated in the present study are included in the figures and/or tables of this article.

Authors' contributions

All authors contributed to the study conception and design. LS was responsible for conceptualization, data curation, formal analysis, investigation, methodology, validation and writing the original draft. PX was responsible for conceptualization, data curation, formal analysis, investigation, methodology, visualization and writing the original draft. AJ was responsible for data curation, investigation, methodology and validation. XX was responsible for validation and visualization. LM was responsible for data curation and investigation. ZW was responsible for methodology. YC was responsible for validation. SW was responsible for software. ST was responsible for formal analysis. DY was responsible for data curation. ZL was responsible for validation. XT was responsible for project administration and supervision. SL was responsible for conceptualization, funding acquisition, project administration, supervision, writing, reviewing and editing. LS and SL

confirm the authenticity of all the raw data. All authors read and approved the final manuscript.

Ethics approval and consent to participate

The present study was performed in line with the principles of the Declaration of Helsinki. The study was approved by the Clinical Ethics Committee of the Affiliated Hospital of North Sichuan Medical College (approval no. 2024020). Animal experiments were performed according to the principles and procedures approved by the Animal Experimentation Ethics Committee of Affiliated Hospital of North Sichuan Medical College (approval no. 202410171). Informed consent was obtained from all individual participants included in the study.

Patient consent for publication

Not applicable.

Competing interests

The authors declare that they have no competing interests.

References

1. Ostrom QT, Price M, Neff C, Cioffi G, Waite KA, Kruchko C and Barnholtz-Sloan JS: CBTRUS statistical report: Primary brain and other central nervous system tumors diagnosed in the united states in 2015-2019. Neuro Oncol 24 (Suppl 5): v1-v95, 2022.
2. Obrador E, Moreno-Murciano P, Oriol-Caballo M, López-Blanch R, Pineda B, Gutiérrez-Arroyo JL, Loras A, Gonzalez-Bonet LG, Martinez-Cadenas C, Estrela JM and Marqués-Torrejón MÁ: Glioblastoma therapy: Past, present and future. Int J Mol Sci 25: 2529, 2024.
3. Zhou M, Li S and Huang C: Physiological and pathological functions of circular RNAs in the nervous system. Neural Regen Res 19: 342-349, 2024.
4. Pisignano G, Michael DC, Visal TH, Pirlog R, Ladomery M and Calin GA: Going circular: History, present, and future of circRNAs in cancer. Oncogene 42: 2783-2800, 2023.
5. Jagtap U, Anderson ES and Slack FJ: The emerging value of circular noncoding RNA research in cancer diagnosis and treatment. Cancer Res 83: 809-813, 2023.
6. Gao Y, Xu L, Sun R, Gao L, Yan P, Yang X, Wang G, Xian Y, Zhang J and Zhu D: Circular RNAs in cancer: Its biogenesis, functions, relationships with cancer progression, applications in immunotherapy and biomarker potentials. Cancer Immunol Immunother 75: 125, 2026.
7. Wang X, Yu L, Qian X and Yu Z: A ESRP1/circPHGDH/miR-149/RAP1B positive feedback loop promotes the malignant behaviors and glycolysis of prostate cancer cell. Exp Mol Med 58: 622-635, 2026.
8. Zhu M, Dong X, Zhang N, Huang N, Zhu Z and Ma J: The circTIMP2/miR-106a/TIMP2 tumor-suppressive axis versus tumor-derived exosomal counteraction in gastric cancer. Apoptosis 31: 106, 2026.
9. Li W, Liu JQ, Chen M, Xu J and Zhu D: Circular RNA in cancer development and immune regulation. J Cell Mol Med 26: 1785-1798, 2022.
10. Wang S, Talukder A, Cha M, Li X and Hu H: Computational annotation of miRNA transcription start sites. Brief Bioinform 22: 380-392, 2021.
11. Ding J, Li X and Hu H: MicroRNA modules prefer to bind weak and unconventional target sites. Bioinformatics 31: 1366-1374, 2015.
12. Bartel DP: MicroRNAs: Genomics, biogenesis, mechanism, and function. Cell 116: 281-297, 2004.
13. Ghazimoradi MH and Babashah S: The role of CircRNA/miRNA/mRNA axis in breast cancer drug resistance. Front Oncol 12: 966083, 2022.
14. Misir S, Wu N and Yang BB: Specific expression and functions of circular RNAs. Cell Death Differ 29: 481-491, 2022.
15. Zhang L, Zhang Y, Gao H, Li X and Li P: Underlying mechanisms and clinical potential of circRNAs in glioblastoma. Oncol Res 31: 449-462, 2023.
16. Li B, Chen J, Wu Y, Luo H and Ke Y: Decrease of circARID1A retards glioblastoma invasion by modulating miR-370-3p/TGFBR2 pathway. Int J Biol Sci 18: 5123-5135, 2022.
17. Kalluri R and LeBleu VS: The biology, function, and biomedical applications of exosomes. Science 367: eaau6977, 2020.
18. Arya SB, Collie SP and Parent CA: The ins-and-outs of exosome biogenesis, secretion, and internalization. Trends Cell Biol 34: 90-108, 2024.
19. van Niel G, D'Angelo G and Raposo G: Shedding light on the cell biology of extracellular vesicles. Nat Rev Mol Cell Biol 19: 213-228, 2018.
20. Paskeh MDA, Entezari M, Mirzaei S, Zabolian A, Saleki H, Naghdi MJ, Sabet S, Khoshbakht MA, Hashemi M, Hushmandi K, *et al*: Emerging role of exosomes in cancer progression and tumor microenvironment remodeling. J Hematol Oncol 15: 83, 2022.
21. Wang W, Sun H, Duan H, Sheng G, Tian N, Liu D and Sun Z: Isolation and usage of exosomes in central nervous system diseases. CNS Neurosci Ther 30: e14677, 2024.
22. Yue M, Hu S, Sun H, Tuo B, Jia B, Chen C, Wang W, Liu J, Liu Y, Sun Z and Hu J: Extracellular vesicles remodel tumor environment for cancer immunotherapy. Mol Cancer 22: 203, 2023.
23. Han QF, Li WJ, Hu KS, Gao J, Zhai WL, Yang JH and Zhang SJ: Exosome biogenesis: Machinery, regulation, and therapeutic implications in cancer. Mol Cancer 21: 207, 2022.
24. Zhang S, Guan N, Mao X, Cui J, Sui X and Guo W: Exosomal circRNA_104948 enhances the progression of glioma by regulating miR-29b-3p and DNMT3B/MTSS1 Signaling. J Environ Pathol Toxicol Oncol 41: 47-59, 2022.
25. WHO Classification of Tumors Editorial Board: Central Nervous System Tumors. WHO Classification of Tumors, 5th edition, Vol. 6. International Agency for Research on Cancer, Lyon, 2021.
26. Livak KJ and Schmittgen TD: Analysis of relative gene expression data using real-time quantitative PCR and the 2(-Delta Delta C(T)) method. Methods 25: 402-408, 2001.
27. Zhang J, Zhang J, Qiu W, Zhang J, Li Y, Kong E, Lu A, Xu J and Lu X: MicroRNA-1231 exerts a tumor suppressor role through regulating the EGFR/PI3K/AKT axis in glioma. J Neurooncol 139: 547-562, 2018.
28. Wang H, Wu J, Luo WJ and Hu JL: Low expression of miR-1231 in patients with glioma and its prognostic significance. Eur Rev Med Pharmacol Sci 22: 8399-8405, 2018.
29. Zhang Z, Yang X, Zheng R, Zang Y, Chen Q, Hu B, Liu M, Liu Y, Huang J, Liang T and Zhang Q: Postoperative exosomal miR-1246 fuels hepatocellular carcinoma metastasis via BMP9-SMAD7 axis suppression. Cancer Lett 648: 218469, 2026.
30. Lang A, Buerger S, Mager L, Erjavc L, Kiesel B, Madlener S, Jaunecker CN, Pacher L, Robert FC, Krausgruber L, *et al*: Tumor-suppressive role of miR-216b impacts cell cycle regulation in high-grade glioma. Acta Neuropathol Commun 14: 81, 2026.
31. Ren QX, Liu YJ, Wang P, Song X, Zhao Q, Cao YN, Hui RT, Yang HT, Zhu Y, Wei CC, *et al*: miR-221 mediates the regulation of phospholamban expression and cardiac contractility by ZBTB20. Acta Physiol (Oxf) 242: e70217, 2026.
32. Li C, Guan X, Jing H, Xiao X, Jin H, Xiong J, Ai S, Wang Y, Su T, Sun G, *et al*: Circular RNA circBFAR promotes glioblastoma progression by regulating a miR-548b/FoxM1 axis. FASEB J 36: e22183, 2022.
33. Shi L, Cao Y, Yuan W, Guo J and Sun G: Exosomal circRNA BTG2 derived from RBP-J overexpressed-macrophages inhibits glioma progression via miR-25-3p/PTEN. Cell Death Dis 13: 506, 2022.
34. Liu X, Guo Q, Gao G, Cao Z, Guan Z, Jia B, Wang W, Zhang K, Zhang W, Wang S, *et al*: Exosome-transmitted circCABIN1 promotes temozolomide resistance in glioblastoma via sustaining ErbB downstream signaling. J Nanobiotechnology 21: 45, 2023.
35. Li Y, Zheng X, Wang J, Sun M, Li D, Wang Z, Li J, Li Y and Liu Y: Exosomal circ-AHCY promotes glioblastoma cell growth via Wnt/β-catenin signaling pathway. Ann Clin Transl Neurol 10: 865-878, 2023.
36. Liu L, Xiao S, Wang Y, Zhu Z, Cao Y, Yang S, Mai R and Zheng Y: Identification of a novel circular RNA circZNF652/miR-486-5p/SERPINE1 signaling cascade that regulates cancer aggressiveness in glioblastoma (GBM). Bioengineered 13: 1411-1423, 2022.

37. Liu R, Dai W, Wu A and Li Y: CircCDC45 promotes the malignant progression of glioblastoma by modulating the miR-485-5p/CSF-1 axis. BMC Cancer 21: 1090, 2021.
38. Balandeh E, Mohammadshafie K, Mahmoudi Y, Hossein Pourhanifeh M, Rajabi A, Bahabadi ZR, Mohammadi AH, Rahimian N, Hamblin MR and Mirzaei H: Roles of Non-coding RNAs and Angiogenesis in Glioblastoma. Front Cell Dev Biol 9: 716462, 2021.
39. Guo Y, Guo Y, Chen C, Fan D, Wu X, Zhao L, Shao B, Sun Z and Ji Z: Circ3823 contributes to growth, metastasis and angiogenesis of colorectal cancer: Involvement of miR-30c-5p/TCF7 axis. Mol Cancer 20: 93, 2021.
40. Yuan F, Zhang S, Sun Q, Ye L, Xu Y, Xu Z, Deng G, Zhang S, Liu B and Chen Q: Hsa_circ_0072309 enhances autophagy and TMZ sensitivity in glioblastoma. CNS Neurosci Ther 28: 897-912, 2022.
41. Liang G, Ling Y, Mehrpour M, Saw PE, Liu Z, Tan W, Tian Z, Zhong W, Lin W, Luo Q, *et al*: Autophagy-associated circRNA circCDYL augments autophagy and promotes breast cancer progression. Mol Cancer 19: 65, 2020.
42. Chen Z, Song J, Xie L, Xu G, Zheng C, Xia X, Lu F, Ma X, Zou F, Jiang J and Wang H: N6-methyladenosine hypomethylation of circGPATCH2L regulates DNA damage and apoptosis through TRIM28 in intervertebral disc degeneration. Cell Death Differ 30: 1957-1972, 2023.
43. Liu Y, Yang Y, Xu C, Liu J, Chen J, Li G, Huang B, Pan Y, Zhang Y, Wei Q, *et al*: Circular RNA circGlis3 protects against islet β-cell dysfunction and apoptosis in obesity. Nat Commun 14: 351, 2023.
44. Zhang ZH, Wang Y, Zhang Y, Zheng SF, Feng T, Tian X, Abudurexiti M, Wang ZD, Zhu WK, Su JQ, *et al*: The function and mechanisms of action of circular RNAs in Urologic Cancer. Mol Cancer 22: 61, 2023.
45. Rong Z, Xu J, Shi S, Tan Z, Meng Q, Hua J, Liu J, Zhang B, Wang W, Yu X and Liang C: Circular RNA in pancreatic cancer: A novel avenue for the roles of diagnosis and treatment. Theranostics 11: 2755-2769, 2021.
46. Fu B, Liu W, Zhu C, Li P, Wang L, Pan L, Li K, Cai P, Meng M, Wang Y, *et al*: Circular RNA circBCBM1 promotes breast cancer brain metastasis by modulating miR-125a/BRD4 axis. Int J Biol Sci 17: 3104-3117, 2021.
47. Zhang C, Ma L, Niu Y, Wang Z, Xu X, Li Y and Yu Y: Circular RNA in lung cancer research: Biogenesis, functions, and roles. Int J Biol Sci 16: 803-814, 2020.
48. Xu K, Ding L, Chang TC, Shao Y, Chiang J, Mulder H, Wang S, Shaw TI, Wen J, Hover L, *et al*: Structure and evolution of double minutes in diagnosis and relapse brain tumors. Acta Neuropathol 137: 123-137, 2019.
49. Jiang Y, Zhao J, Li R, Liu Y, Zhou L, Wang C, Lv C, Gao L and Cui D: CircLRFN5 inhibits the progression of glioblastoma via PRRX2/GCH1 mediated ferroptosis. J Exp Clin Cancer Res 41: 307, 2022.
50. Long N, Xu X, Lin H, Lv Y, Zou S, Cao H, Chen X, Zhao Y, Qi X, Yang H, *et al*: Circular RNA circPOSTN promotes neovascularization by regulating miR-219a-2-3p/STC1 axis and stimulating the secretion of VEGFA in glioblastoma. Cell Death Discov 8: 349, 2022.
51. Zou Y, Zheng S, Xiao W, Xie X, Yang A, Gao G, Xiong Z, Xue Z, Tang H and Xie X: circRAD18 sponges miR-208a/3164 to promote triple-negative breast cancer progression through regulating IGF1 and FGF2 expression. Carcinogenesis 40: 1469-1479, 2019.
52. Zhong Y, Du Y, Yang X, Mo Y, Fan C, Xiong F, Ren D, Ye X, Li C, Wang Y, *et al*: Circular RNAs function as ceRNAs to regulate and control human cancer progression. Mol Cancer 17: 79, 2018.
53. Yang Q, Li F, He AT and Yang BB: Circular RNAs: Expression, localization, and therapeutic potentials. Mol Ther 29: 1683-1702, 2021.
54. Zhu L, Zhang K, Zhang C, Yu H and Zhu L: Low miR-1231 expression predicts poor prognosis in non-small-cell lung cancer and accelerates cell proliferation, migration and invasion. Biomark Med 15: 831-840, 2021.
55. Jourdain AA, Begg BE, Mick E, Shah H, Calvo SE, Skinner OS, Sharma R, Blue SM, Yeo GW, Burge CB and Mootha VK: Loss of LUC7L2 and U1 snRNP subunits shifts energy metabolism from glycolysis to OXPHOS. Mol Cell 81: 1905-1919.e12, 2021.
56. Douet-Guilbert N, Soubise B, Bernard DG and Troadec MB: Cytogenetic and genetic abnormalities with diagnostic value in myelodysplastic syndromes (MDS): Focus on the Pre-messenger RNA splicing process. Diagnostics (Basel) 12: 1658, 2022.
57. Shen L, Li C, Chen F, Shen L, Li Z and Li N: CRISPR/Cas9 genome-wide screening identifies LUC7L2 that promotes radioresistance via autophagy in nasopharyngeal carcinoma cells. Cell Death Discov 7: 392, 2021.
58. Yue Q, Wang Z, Shen Y, Lan Y, Zhong X, Luo X, Yang T, Zhang M, Zuo B, Zeng T, *et al*: Histone H3K9 lactylation confers temozolomide resistance in glioblastoma via LUC7L2-Mediated MLH1 Intron retention. Adv Sci (Weinh) 11: e2309290, 2024.
59. Zhang L and Yu D: Exosomes in cancer development, metastasis, and immunity. Biochim Biophys Acta Rev Cancer 1871: 455-468, 2019.
60. Roma-Rodrigues C, Fernandes AR and Baptista PV: Exosome in tumour microenvironment: Overview of the crosstalk between normal and cancer cells. Biomed Res Int 2014: 179486, 2014.
61. Zhou WY, Cai ZR, Liu J, Wang DS, Ju HQ and Xu RH: Circular RNA: metabolism, functions and interactions with proteins. Mol Cancer 19: 172, 2020.
62. Li P, Xu Z, Liu T, Liu Q, Zhou H, Meng S, Feng Z, Tang Y, Liu C, Feng J, *et al*: Circular RNA sequencing reveals serum exosome circular RNA Panel for High-grade astrocytoma diagnosis. Clin Chem 68: 332-343, 2022.
63. Wang S, Zhang K, Tan S, Xin J, Yuan Q, Xu H, Xu X, Liang Q, Christiani DC, Wang M, *et al*: Circular RNAs in body fluids as cancer biomarkers: The new frontier of liquid biopsies. Mol Cancer 20: 13, 2021.